UNIVERSITI TEKNOLOGI MARA

THOMSON AND TROIAN SLIP ON MAGNETOHYDRODYNAMIC (MHD) FLOW OF EYRING-POWELL TERNARY NANOFLUID PAST A STRETCHING/SHRINKING SHEET

NUR NATASHA BINTI SARBANI

BACHELOR OF SCIENCE (HONS.) MATHEMATICAL MODELLING AND ANALYTICS

FACULTY OF COMPUTER AND MATHEMATICAL SCIENCES

JULY 2025

APPROVED BY:

DR. NUR SYAZANA ANUAR

Supervisor

Faculty of Computer and Mathematical Sciences

Universiti Teknologi MARA

ABSTRACT

The purpose of this study is to examine the flow of an Eyring-Powell ternary nanofluid under the influence of magnetic parameter, volume fraction of nanoparticles, Thomson and Troian slip condition over both shrinking and stretching surfaces. The governing equations which are equations of momentum, continuity, and energy along with its boundary conditions were formulated. The partial differential equation of the system was transformed into ordinary differential equation using the similarity variables before being solved numerically using the MATLAB's built-in software, BVP4C. The present results were validated through comparison with past studies, showing a good accuracy of the current model. The impact of different values of volume fraction of nanoparticles, magnetic, slip velocity and critical shear rate parameters on local skin friction, Nusselt number, velocity and temperature profile were analysed and illustrated graphically. The results reveal that the velocity profile and Nusselt number increases while the temperature profile decreases when the value of magnetic, slip velocity and critical shear rate parameter increases. Local skin friction becomes higher with higher value magnetic parameter but lower value of slip velocity and critical shear rate parameters. Furthermore, ternary nanofluid exhibit the lowest velocity but the highest temperature and local skin friction compared to hybrid nanofluid and nanofluid while ternary nanofluid shows a moderate Nusselt number.

ACKNOWLEDGEMENT

Firstly, I want to thank Allah for giving me the opportunity to complete my research for the Final Year Project. I am truly grateful that I am able to complete my project with good health be it physically and mentally. I wish to express my gratitude to my supervisor, Dr. Nur Syazana Anuar, for her unwavering encouragement and full guidance and suggestions throughout my project. The guidance was really helpful and improved my comprehension of the topic.

Next, I would like to thank my parents for their full support and for always encouraging me by giving the motivation to finish this project. Not to mention, special thanks to my classmate for always being there for me and sharing their thoughts for the projects. The project might not be finished without their assistance. Lastly, I would like to express my deepest appreciation to the people that are directly or indirectly helping me in this report completion.

TABLE OF CONTENTS

LIST OF TABLES

LIST OF FIGURES

LIST OF SYMBOLS

τ_w	Shear Stress
μ	Dynamic viscosity
δ_x	Boundary layer thickness
β_1	Eyring-Powell fluid parameter
E_1	Eyring-Powell fluid parameter
u, v	Velocity components along x - and y -axes
u_w	Velocity at the wall in
u_t	Tangential velocity
B	Magnetic field
T	Temperature
T_∞	Ambient temperature
T_w	Temperature at the wall
ρ	Density
σ	Electrical conductivity
k	Thermal conductivity
C_p	Specific heat
C_f	Skin friction coefficient
γ^*	Navier slip length
ξ^*	Reciprocal of shear rate
S	Suction/injection parameter
ϕ_1	Volume fraction of nanoparticle AA7072
ϕ_2	Volume fraction of nanoparticle AA7075
ϕ_3	Volume fraction of nanoparticle $CoFe_2O_4$
(ρC_p)	Heat capacity

Nu_x	Nusselt Number
q_w	Surface heat flux
v_f	Kinematic viscosity
η	Similarity variable
f	Dimensionless stream function
θ	Dimensionless temperature
M	Fluid parameter
Pr	Prandtl number
λ	Shrinking/Stretching parameter
λ_c	Critical shrinking/Stretching parameter
L_1	Velocity slip parameter
L_2	Critical shear rate parameter
Re_x	Reynold number
a, n^*	Constant

LIST OF ABBREVIATIONS

MHD	Magnetohydrodynamic
PDE	Partial differential equation
ODE	Ordinary differential equation
TD	Tiwari and Das
RKF45	Runge-Kutta-Fehlberg method

LIST OF SUBSCRIPTS

thnf	Ternary nanofluid
hnf	Hybrid nanofluid
nf	Nanofluid
bf	Base fluid

CHAPTER 1
INTRODUCTION

1.1 Research Background

Boundary layer is a thin layer of flowing fluid that forms when in contact with a solid surface and the development of a boundary layer is illustrated in Figure 1. This theory is introduced by Ludwig Prandtl in 1904. The boundary layers are typically classified into two types which are laminar and turbulent boundary layer. The horizontal axis, which is the distance of the plate is labelled as x, while the distance perpendicular to the plate is y. As the fluid flows over the surface, a boundary layer forms where the velocity changes from zero to freestream velocity, U_∞ and the velocity inside the boundary layer is denoted as $u(x, y)$ while δ_x represents the boundary layer thickness. The laminar boundary layer, which typically occurs at low velocities, is when the fluid flows smoothly and the particles are arranged in parallel layers (Schlichting & Gersten, 2016). However, in turbulent boundary layer, the flow is more chaotic than in the laminar flow, improving the fluid's heat transfer ability.

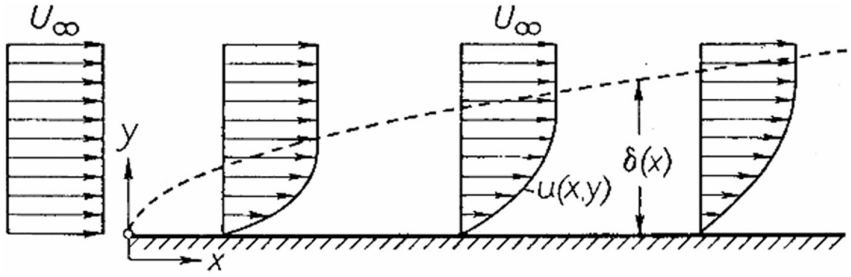

Figure 1. Boundary Layer (Schlichting & Gersten, 2016)

The transition of the laminar to turbulent boundary layer is caused by an unstable flow and a disturbance that occurs in the stream outside of the layer. During the transition region, the layer gradually becomes unstable and separated from the layer, which later rejoins as the turbulent layer (De Vault et al., 1939) as depicted in Figure 2. The separation point of the boundary layer occurs when the fluid starts to detach from the wall (Smith, 1986). One of the causes are due to the adverse pressure gradient around the surface (Simpson, 1989). Adverse pressure gradient is when there are increases in pressure in the direction of the flow. (Kundu et al., 2016).

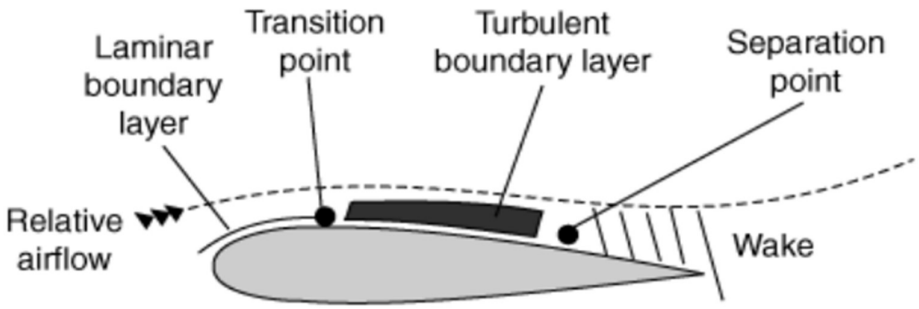

Figure 2. Separation point of boundary layer (Chalia & Bharti, 2017)

There are two main categories of fluids which are Newtonian fluids and non-Newtonian fluids. They are distinguished by their viscosity, or the measure of its resistance to shear stress applied on the fluid. Newtonian fluids are defined as those whose viscosity does not change in response and independent to applied stress and that are not affected by shear stress. For example, water, and alcohol. On the other hand, non-Newtonian fluids have a non-linear relationship with shear stress and strain, and its viscosity does not remain constant after some external force. Unlike Newtonian fluids, the fluids may become more thicker or thinner. Custard, starch and blood are a few examples (Böhme, 2012). Non-Newtonian fluid is widely used in the industry as they have complex behaviours that make them suitable for various process.

As non-Newtonian exhibit a complex behaviour compared to the normal fluid, models are used to describe their characteristics using equations to gain more understanding of it. Some of the examples of non-Newtonian models are Ellis Fluid Model, Power Law, that shows the simple relationship between shear stress and shear rate (Chhabra, 2010), and Eyring-Powell model with the equation of shear tensor, $\tau_{ij} = \mu \frac{\partial u_i}{\partial x_j} + \frac{1}{\beta} \sinh^{-1}\left(\frac{1}{E}\frac{\partial u_i}{\partial x_j}\right)$, where τ_{ij} is the shear tensor, E and β is the Eyring-Powell fluid parameters, and μ refers to dynamic viscosity. Eyring-Powell model has several advantages over other models such as; the model was not derived from the empirical connection but rather from the kinetic theory of liquids. Then, for both low and high shear rates, it accurately reduces to Newtonian behaviour (Rahimi et al., 2017). By examining how these fluids behave under shear strain, the Eyring-Powell model aids in industry design and application optimization.

Nanofluid is a fluid that is made of nano-sized particles is discovered by Choi in 1995 for the improvement of thermal properties of fluid due to higher energy demands (Zheng & Zhang, 2017). By mixing in the base fluid with small amounts of solid particles, the heat transfer ability of the fluid is enhanced, making it useful in the applications such as engine cooling and chiller (Chamsa-ard et al., 2017). Hybrid nanofluid is when more than one nanoparticle is added. It was introduced to overcome the higher demand of the industry. It has stronger heat conduction mechanism as they are capable to cool down systems with high temperatures. For example, ternary nanofluid is made up from the suspensions of three different nanoparticles into the base liquid. The presence of multiple nanoparticles in ternary nanofluids enhance its properties such as the thermal conductivity and are more efficient in heat transfer through convection (Adun et al., 2021).

A no-slip condition in fluid dynamics states that the velocity of the fluid that is in contact with the surface is zero as displayed in Figure 3. However, non-Newtonian fluids often exhibit a slip condition, which is the velocity of the fluid that is closest to the solid is non-zero. The cause for this condition is due to the surface roughness as it can influence the movement of the fluid along the surface (Sochi, 2011). When the surface is rougher, the slip that occur will decrease and the non-zero velocity of the fluid near the surface can help carry the heat faster away from the solid, making the heat transfer process more efficient.

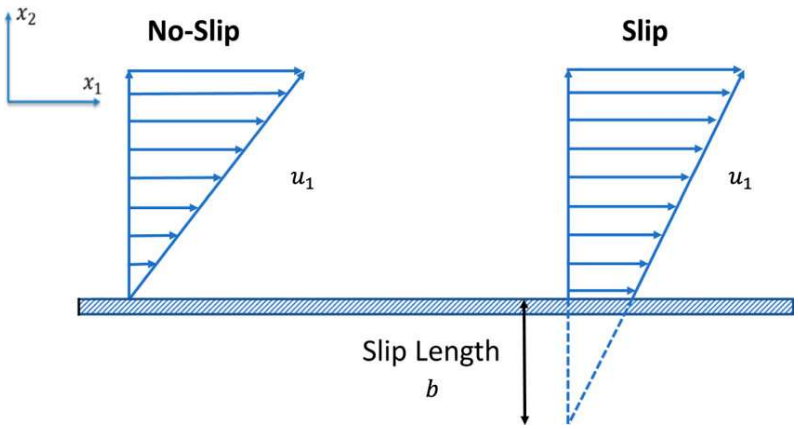

Figure 3. Slip and no-slip condition (Uthe et al., 2022)

Some of the models are introduced to describe the slip condition which are Navier slip and Maxwell slip condition. However, for more generalised slip condition, Thomas and Troian

slip are introduced where the length of the slip does not stay constant but can varies with shear rate. In this model, the slip length becomes a variable since it can be different when the shear rate is increasing (Dey et al., 2023). Thomson and Troian slip condition involves a non-linear relationship of the shear rate which is different from Navier slip that consider the linear relationship of the slip velocity and the shear rate (Singh et al., 2024).

Magnetohydrodynamics (MHD) is a study of the fluid dynamics in the presence of a magnetic field and the word magnetohydrodynamics is derived from the word magneto, hydro and dynamics. Salt water, liquid metals and plasmas are some of the examples for electrically conducting fluids. Forces on the fluid is created by the currents in the fluid that is instigated by the magnetic field (Sheikholeslami & Ganji, 2016). Examples for the applications of MHD are magnetic endoscopy and transporting complex bio-waste fluids. The presence of the magnetic field has a significant influence on the heat transfer ability of the fluid.

1.2 Motivation

In this modern world where advanced technology has been developed, the demand for better thermal conductivity and heat transfer ability has been increasing. The high-performance technology that produces a lot of heat can cause overheating which will reduce its efficiency and can cause internal damage. Hence, cooling systems are important to this technology as it can prevent overheating and extend its lifespan. Nanofluids have been used widely in the industry in the cooling system as it has higher thermal conductivity and can transfer heat better, especially ternary nanofluid where it contains a combination of 3 types of nanoparticles that enhances its heat transfer ability. Then, by considering the effect of the magnetohydrodynamic effects, it can improve the understanding of applications that involves the presence of magnetic field. Although no-slip conditions are a common assumption, slip effects may occur particularly in a high-shear system and it should be considered to develop a more accurate mathematical model to the real-world. This study is motivated by the research gap as there is limited studies that studied simultaneously on the effects of the magnetic field and Thomson and Troian slip condition on Eyring-Powell ternary nanofluid flow over stretching/shrinking sheet due to the complexity of the non-Newtonian behavior and the nonlinear slip conditions. This study will observe the effects of these parameters which will help to develop a better cooling system of the industry by understanding their behavior and gain more insight about advance fluid dynamics.

1.3 Problem Statement

Nanofluid is an enhanced fluid that has improved thermal conductivity, heat capacity, electrical conductivity and is a great thermal transport. It was widely used in the industry where heat transfer is important such as on heating or cooling applications (Aich et al., 2023). However, although the nanofluids have helped the industry tremendously, there are still some challenges faced such as the effectiveness, stability, and the production cost of it (Saidur et al., 2011). The standard nanofluid that only contains one type of nanoparticle has a limited thermal conductivity for applications in the industry that are in need for greater heat transfer ability. To overcome these limitations, new nanoparticles such as hybrid nanofluid, that are more advanced and specialize in suiting their needs and have higher thermal conductivity are introduced.

Then, the study of magnetohydrodynamic (MHD) is important as the use of nanofluids that is electrically conducting fluids due to its metal nanoparticles can influence the boundary layer flow. Some of the cooling rectors in industry such as nuclear reactor cooling channels, do depend on the magnetic field as electrically conducting nanofluid is widely used as it can help to enhance the heat transfer efficiency (Ishak, 2011). Furthermore, no-slip condition is commonly assumed from various previous studies, however, small slips may occur which will affect the velocity of the fluid on the surface and its heat transfer. The Thomson and Troian slip where the slip varies with the local shear stress, making it more accurate for high shear flow applications, has not been extensively studied and the presence of slip improves the fluids flow efficiency (Ramzan et al., 2020).

Therefore, this study focuses on the magnetohydrodynamic (MHD) Eyring-Powell ternary nanofluid that consists of engine oil as its base fluid with aluminium alloys (AA7072 and AA7075) and cobalt ferrite nanoparticles, with Thomson and Troian slip condition.

1.4 Research Objectives

The objectives of this study are:

i. To formulate a mathematical model of boundary layer flow of magnetohydrodynamic (MHD) Eyring-Powell ternary nanofluid over a stretching/shrinking sheet with Thomson and Troian slip condition.

ii. To transform partial differential equation (PDE) into nonlinear ordinary differential equation (ODE) by using similarity transformation method.

iii. To solve the ordinary differential equation (ODE) using BVP4C solver in MATLAB software.

iv. To analyse the impact of magnetic field, critical shear rate, velocity slip parameter and volume fraction of nanoparticle on velocity and temperature profile, and skin friction coefficient and local Nusselt number.

1.5 Significance of Study

The significance of this study is by understanding the properties of the nanoparticle and its composition, we can use the nanoparticle to its maximum potential which will improve its performance in the industry, Eyring Powell model captures shear-dependent viscosity behavior at both low and high shear rates, making it more significant than the other models. This study uses mathematical modelling as it has lower cost rather than doing a physical experiment that requires nanoparticles which are more time consuming and have higher cost. This model can also be used for predictions when there are changes in any of the variables. It will improve the prediction of the systems and help to advance the industry, making the uses of these nanofluid to be optimized.

The new nanofluids are introduced to further enhance their effectiveness in the industry. They have been modified to a more advanced nanofluid that specializes in a specific application, making it more effective. The presence of different types of nanoparticles in a base fluid can improve the properties of the fluid. In this study, the nanoparticles are aluminium alloys (AA7072 and AA7075) and cobalt ferrite ($CoFe_2O_4$) in a base fluid of an engine oil. These nanoparticles increase the thermal and mechanical properties. By modelling this fluid behaviour under the influence of magnetic parameter and slip condition, it can provide insights of its behaviour which can lead to improved systems such as cooling technologies and even lubr.

1.6 Limitation

This study has some limitations which are, the results obtained are solved numerically using the MATLAB software and BVP4C solver. This research is not done experimentally, which

may have a different result with the real practical systems. The mathematical model formulated in this study does not completely represent the complex real-world system as it has been simplified by omitting some factors and only considering multiple parameters as a complex model is time consuming and more challenging. The simplifications of the model may affect the model predictive ability for the applications.

1.7 Assumption

In this study, some assumptions are made to simplify the mathematical model. This study assumed the flow to be laminar and steady. Then, nanoparticles are assumed to be uniformly distributed across the base fluid. The magnetic field is applied vertically to the stretching/shrinking sheet. Moreover, Thomson and Troian slip condition is assumed to be present where the local shear stress causes the slip length to vary. Although these assumptions were made to simplify the model, it is still relevant to analyse the impacts of magnetic parameter, velocity slip and critical shear rate parameters, and the volume fraction of the nanoparticles to the velocity and temperature profiles, local skin friction coefficients and Nusselt number effectively.

1.8 Ethical Committee

UNIVERSITI TEKNOLOGI MARA
Kolej Pengajian Pengkomputeran, Informatik dan Matematik

Our Reference : 100-KPPIM(PI.9/10/)(EX/1660)
Date : 4th June 2025

Dr. Nur Syazana Anuar
Nur Natasha Binti Sarbani (2022646416)
College of Computing, Informatics & Mathematics
Universiti Teknologi MARA
40450 Shah Alam
SELANGOR

Dear Dr.,

ETHICS REVIEW EXEMPTION - COLLEGE ETHICS REVIEW COMMITTEE

Thank you for submitting your research proposal to the College Ethics Review Committee (CERC). After considering your application, the Committee approved your proposal entitled **"THOMSON AND TROIAN SLIP ON MAGNETOHYDRODYNAMIC (MHD) FLOW OF EYRING-POWELL TERNARY NANOFLUID PAST A STRETCHING/SHRINKING SHEET"** is exempted from ethics review.

Details of the ethics review exemption are as follows:

Ref. number:	100-KPPIM(PI.9/10/)(EX/1660)
Authorised personnel:	1. DR. NUR SYAZANA ANUAR 2. NUR NATASHA BINTI SARBANI (2022646416)

The College Ethics Review Committee operates in accordance with the ICH Good Clinical Practice Guidelines, Malaysian Good Clinical Practice Guidelines and the Declaration of Helsinki. The approval of this project is conditional upon your continuing compliance with these guidelines and declaration.

If you require further information, please contact CERC Secretariat at 03-7962 2006 or email at afiqahhamid@uitm.edu.my.

Yours sincerely,

DR. JASBER KAUR A/P GIAN SINGH
Chairman
College Ethics Review Committee, KPPIM

Kompleks Al-Khawarizmi
Universiti Teknologi MARA
40450 Shah Alam, Selangor Darul Ehsan
MALAYSIA
Tel: (+603) 5543 5329 / 5305
Faks: (+603) 5543 5501

1.9 Thesis Scope

This research focuses on the steady and laminar part of the boundary layer flow rather than the unsteady effects. Furthermore, only some parameters are considered in the formulation which are magnetic, slip parameters and volume fraction of nanoparticles. Other parameters such as thermal radiation and chemical reaction are not considered. Then, the nanoparticles used in this study are aluminium alloys (AA7072 and AA7075) and cobalt ferrite ($CoFe_2O_4$) with the base fluid engine oil while the other combinations of nanoparticles were not being studied. The influence of different nanoparticles was not considered which may be needed in different real-life applications. Future work can consider these aspects to develop a more accurate and realistic model.

1.10 Thesis Outline

This research consists of five chapters which are introduction, literature review, methodology, results and discussion, then conclusion. In the first chapter, introduction, the background of the study is explained, related to the boundary layer flow, nanofluid, Eyring-Powell model, magnetohydrodynamic, and Thomson and Troian slip condition. This chapter consists of motivation, problem statements, research objectives, research questions, significance of the study, limitation, assumption, ethical committee, and thesis scope. Then, Chapter 2 provides the literature review of the previous research that involves the topics of boundary layer flow of Eyring-Powell fluid, boundary layer, hybrid nanofluid, boundary layer flow with Thomson and Troian velocity slip, boundary layer flow with the magnetohydrodynamic (MHD) effect and identifies the research gap.

Chapter 3 describes the methodology of this research, where it starts with mathematical formulation, transforming partial differential equations (PDEs) into ordinary differential equations (ODEs) through the similarity transformation. The ODEs were then solved numerically using the MATLAB built-in software, BVP4C. In Chapter 4, results and discussion, the numerical values obtained are validated with several past research and the impact of magnetic parameter, velocity slip and critical shear rate parameter, and volume fraction of nanoparticles on velocity profile, temperature profile, local skin friction and Nusselt number

were illustrated graphically and discussed. Finally, Chapter 5 concluded the key findings of the study and recommendations for future study were provided.

CHAPTER 2

LITERATURE REVIEW

2.1 Boundary Layer Flow on Eyring Powell

There are numerous authors that have done research about boundary layer flow on Eyring Powell. Patel & Timol (2009) did a study about the Eyring-Powell fluid flow where the two-dimensional flow equations are solved by the method of satisfaction of asymptotic boundary conditions. Javed et al. (2013) also did research of Eyring-Powell fluid flow on a stretching sheet where the higher value of fluid parameter will lower the velocity profile. Hayat et al. (2013) extended the study by considering the convective boundary conditions of the Eyring-Powell flow over a stretching sheet and the differential systems were solved using homotopy method. It was found that the boundary layer thickness and the temperature decrease by the fluid parameters. Then, Hayat et al. (2015) takes account of the effects by the heat and mass transfer of the flow of three-dimensional Eyring-Powell fluid. The analytical solutions of the problem were obtained by homotopy analysis method. The result gained from this research is that with the increasing of Eyring-Powell parameters, the velocity profile increases.

Sher Akbar et al. (2015) expanded the research by adding the magnetic field effects towards the Eyring-Powell fluid flow over a stretching sheet. This problem was solved using implicit finite difference method and the result obtained is when the Eyring-Powell fluid parameters is increasing, it will cause a stronger resistance of flow. Aside from that, Ishaq et al. (2018) further investigates the effects of magnetohydrodynamic (MHD) on the nanofluid flow of Eyring Powell model over a porous stretching surface. Using the optima approach, the study found that there is a decrease in the system entropy when the fluid parameter is increasing. Pal & Mondal (2022) performed research of the combined effects of magnetic field and buoyancy force, microorganisms and nanoparticles added to the Eyring Powell fluid to make it more stable over the stretching sheet in the presence of thermal radiation. By solving the equations using similarity transformation, it was revealed that with an increase in Eyring-Powell fluid parameter, the microorganisms difference parameter will decrease.

Then, Kumar & Srinivas (2020) considered the chemical reactions and added the effects of Joule heating and thermal radiation to the flow of Eyring-Powell fluid on an inclined stretching sheet. Runge-Kutta fourth order is one of the methods used to obtain the results from the flow equations. It was discovered that when there are increases in Eyring-Powell fluid parameters will cause the increment of the velocity profile while the local skin friction coefficient is higher

due to the increasing radiation parameter. Meanwhile, Naseem et al. (2023) did research about the analysis of heat transport of Eyring Powell model with joule heating effects and radiation by similarity transformation and the result was the temperature profile decreases while the velocity profile increases for a higher value of fluid parameters. Mwamba (2024) expand the study by investigating the flow of Powell-Eyring fluid over a stretching sheet while considering dissipation, thermal radiation and Dufour effects and solve it numerically using bvp4c in MATLAB. He found that with the increasing ratio of velocity, is due to increases of Eyring-Powell fluid parameter while a higher value of magnetic parameter causes the velocity ratio to drop.

2.2 Boundary Layer Flow of Hybrid Nanofluid

Many studies have focused on hybrid nanofluids that are mainly used in industry as they have enhanced heat transfer properties. Hayat & Nadeem (2017) did research about how chemical reaction effects and radiation affect the boundary layer flow of 3D rotation hybrid nanofluid in terms of its heat transfer characteristics over the stretching sheet. In this research, the hybrid nanofluid contains of water as its base fluid with Silver and Copper Oxide nanoparticles. By solving the system using bvp4c technique, they found that the rotation parameter increases the thermal boundary layer thickness and the presence of the hybrid nanofluid causes the temperature of the fluid to rise. Aziz et al. (2020) studied about the effect on the flow and the whole entropy of the Eyring-Powell nanofluid that is caused by the combination of thermal radiation and viscous dissipation and Keller box infinite difference scheme is used to find the solutions. They experimented on two types of nanofluid which are copper water (Cu-H_2O) nanofluid and alumina-copper water (Al_2O_3-Cu/H_2O) hybrid nanofluid and were compared. It was found that hybrid nanofluid (Al_2O_3-Cu/H_2O) is a better thermal insulator than copper water nanofluid and when the concentration of the nanoparticle increases, the rate of the heat transfer also increases.

Then, the study was extended by Ahlam Aljabali et al. (2023) as they added the effect of the radiative heat flux to the flow of the hybrid Eyring-Powell nanofluid over a shrinking sheet and bvp4 function is applied to find the solution. Hybrid nanofluid that is being used is Ag-MgO, which is a water nanofluid and parameters such as shrinking parameter and radiation parameter are used to regulate the performance of the fluid. When the thermal radiation increases, heat distribution enhances and when the concentration of the nanoparticles increases, the heat

transmission is improved. Rashad et al. (2023) expanded the research by considering the flow of magnetic Eyring-Powell hybrid nanofluid that was affected by the heat source in a pored medium and thermal radiation and the method used are RKF45 and shooting method. The hybrid nanofluid contains ethylene glycol (EG), magnetite (Fe_3O_4) and copper (Cu). The thermal rate for the fluid increases due to the resistance to the fluid motion when the magnetic parameter increases, and the temperature rises when the volume of the nanoparticles increases that later cause the increased viscosity of the fluid with its resistance to flow.

The research then furthered by Ramireddy and Lakshmi (2024) where the impact of joule heating, buoyancy driven flow, thermal radiation, velocity profiles and viscous dissipation on the flow of the hybrid nanofluid over a porous cylinder surface is observed and solved using Keller Box method of convergence. The hybrid nanofluid selected for this research is blood as the base fluid where it will be mixed with magnesium (Mg) and magnetite (Fe_3O_4) nanoparticles. The observation confirms that hybrid nanofluid is a better coolant than an ordinary base fluid since hybrid nanofluid can release more heat. On the other hand, Akram et al. (2024) did a study about the peristaltic flow of the hybrid nanofluid through an elliptical conduit where the system is solved using the perturbation technique. Polystyrene and graphene oxide nanoparticles were contained in the hybrid nanofluid with water as its base fluid and it was found that when the elliptic of the conduit reduces into a circular shape, it diminishes the pressure gradient of the system. Then, by increasing the concentration of the nanoparticle, it can enhance the temperature profile of the fluid across the elliptic conduit.

A study was done by Manjunatha et al. (2022) to observe the thermal conductivity between the ternary nanofluid and hybrid nanofluid where the system of equations was solved using RKF-45 method. The result reveals that ternary nanofluid has better heat transfer abilities compared to hybrid nanofluid and nanofluid. However, there are still lack of research on the behavior of the ternary nanofluids on the boundary layer flow.

2.3 Boundary Layer Flow with Thomson and Troian Velocity Slip

Many studies have considered the presence of Thomson and Troian velocity slip condition at the boundary. Abbas et al. (2019) researched about the how the electrically conducting nanofluid is affected by mixed convection and homogeneous-heterogeneous reaction by using the Tiwari and Das (TD) model with the boundary condition of Thomson and Troian over a shrinking and stretching sheets. Some of the parameters used to analyse the model were

volume fraction parameter, slip velocity parameter and critical shear rate parameter. It was found that the temperature profile exhibits distinct changes when being compared using partial slip and generalised slip and the increasing value of critical shear rate parameter and slip velocity parameter decreases the temperature profile. Nonlinear thermal radiation factor was added to the next research by Ahmad & Nadeem (2020) where they explored about water hybrid nanofluid affected by induced magnetic field with Thomson and Troian boundary condition over a nonlinear permeable stretching surface by using Cattaneo-Christov model of heat flux. It was discovered that the skin friction coefficient lowers with higher values of critical shear rate parameter.

Then, Ramzan et al. (2020) extended the study by adding the impact of heat generation and the buoyancy effect to the mathematical model of carbon nanotubes, where both single-wall and multi-wall are considered, contained by the nanofluid over a stretching/shrinking surface near the stagnation point that discussed about the impact of the Thomson and Troian slip boundary. Using bvp4c function in MATLAB, it was found that when the solid values fraction and heat generation increases, the temperature of the system decreases, and the fluid velocity enhances by the slip velocity parameter. Akaje & Olajuwon (2021) further develop the study by using the magnetohydrodynamic (MHD) Casson nanofluid to explore the effect of nonlinear radiative heat transfer with the Thomson and Troian slip boundary condition where the solution is obtained by the spectral collocation method. The result shows that the higher values of thermal radiation and temperature ratio will thicken the temperature boundary layer and by increasing the value of critical shear rate, the temperature profile will be higher.

Dey et al. (2022) took the study further by combining the impact of Thomson and Troian slip and Stefan blowing of nanofluid over a non-absorbent plate on forced convection motion. Numerous parameters were taken account which were suction/blowing, velocity slip, Brownian, and chemical reaction parameters. The result achieved from the numerical solution was the higher value of Stefan blowing parameter reduces the skin friction coefficient and increases the temperature profile while the increasing in critical shear rate and slip parameter causes the rate of mass transport to decrease. On the other hand, research about the flow of ternary nanofluid with the condition of Thomson and Troian were done by Li et al. (2023) to analyse the heat transfer abilities of the nanofluid that is formed from water as a base fluid that consists of Cu, Ag and TiO_2 nanoparticles due to the slip impact. The mathematical model was solved using the RKF-45 method which results in the amount of heat conducted by the fluid to lower due to the higher thermal slip parameter.

Then, Mishra (2024) enhances the study of hybrid nanofluids flow over a surface while suction effects and Thomson and Troian slip are considered by aiming to analyse the nanofluid's hydro-thermal and electromagnetic characteristics, electromagnetohydrodynamic (EMHD) and solved it numerically using bvp4c function. Multiple parameters effects on the temperature distribution are observed which are permeability, heat generation, electric, velocity slip and critical shear rate parameter. The study found that the velocity of the hybrid nanofluid increases due to the rise value of velocity slip, critical shear rate and electric parameter.

2.4 Boundary Layer Flow with Magnetohydrodynamic (MHD) Effect

Magnetohydrodynamic (MHD) can alter the boundary layer flow such as its viscosity and even the fluid's velocity due to the presence of the magnetic and electric current in the fluid. Ibrahim and Tulu (2019) studied the heat and mass transfer of nanofluid encased in the porous surface with viscous dissipation effects and the MHD boundary layer flow that passes through the wedge which will then be solved using the Spectral Quasilinearisation Method. Several parameters and their effects on the velocity, temperature and concentration field are observed and analysed. The result shows that the increase of magnetic parameter and permeability reduces the velocity boundary layer thickness that are caused by the retarding force on the velocity field due to the presence of transverse magnetic field. Then, the study was extended where a study MHD peristaltic flow in the walls that are moving with peristaltic wave velocity was considered with the impact of joule dissipation and variable electrical conductivity by Qasim et al. (2019) by using the Generalised Differential Quadrature Method. The velocity of the temperature profiles decreases in the center of the flow with the increases of the Hartmann number because of the interactions between the magnetic field and the electrically conducting fluid that produces the opposing Lorentz force to the fluid flow direction.

On the other hand, Raza (2019) adds the effects of slip and thermal radiation on the flow of Casson fluid's magnetohydrodynamic stagnation point across a convective heated stretching sheet and were solved using the method of Runge-Kutta-Fehlberg. The rise in value of magnetic parameters causes the rate of the fluid flow to become lower. Then, Fatunmbi et al. (2020) expanded the research about by considering multiple slip conditions of the magnetohydrodynamic fluid flow in a porous medium and the flow, mass, and heat transfer and the impact of the thermal, velocity and concentration boundary conditions over the non-linear surface were observed. Using the spectral quasi-linearisation method, the observation

obtained is velocity of the fluid will decrease while the temperature distribution will increase with the rise of magnetic field.

Lund et al. (2020) refined the research by investigating the stability of the hybrid nanofluid that contains the nanoparticles of Cu-Al_2O_3 with water as its base fluid, carrying out the MHD flow in the presence of thermal radiation across the stretching and shrinking sheet by using the shooting method in Maple software. The result obtained is with the decreases of the volume fraction for nanoparticle copper, the magnetic parameter gets higher which leads to a better heat transfer rate. In a related context, Ullah et al. (2021) explores the MHD blood flow over a stretching surface that is impacted by the thermal conductivity, temperature dependent viscosity, chemical reaction, and ohmic effect where Levenberg-Marquardt scheme-based propagation technique (NN-BLMS) is used. The findings indicate that the electromagnetic force appeared due to the presence of ohmic effect, and the temperature of the blood rises. The flow temperature also becomes higher when the viscous heating in the flow is generated by the magnetic field.

Although there are few studies that investigated the impact of MHD and Thomson and Troian velocity slip on hybrid nanofluid separately, research that considers these two effects, magnetic field, velocity slip and critical shear rate parameters at the same time with Eyring-Powell ternary nanofluids is very limited. Therefore, the study of these parameters impacting the velocity profile, temperature profile, skin friction coefficient and Nusselt number can improve the understanding of how these parameters behave which is crucial for the industry.

CHAPTER 3

RESEARCH METHODOLOGY

3.1 Introduction

This chapter begins with the mathematical formulation which includes continuity, momentum, and energy equations, along with the boundary conditions. This study is extended from the research of Javed et al. (2013) by considering magnetohydrodynamic (MHD) ternary nanofluid with Thomson and Troian velocity slip. The partial differential equations are transformed into ordinary differential equations by using the similarity transformation and then will be solved using BVP4C solver in MATLAB software, gets validated by past research, and the result will be discussed as depicted in the methodology framework as shown in Figure 4.

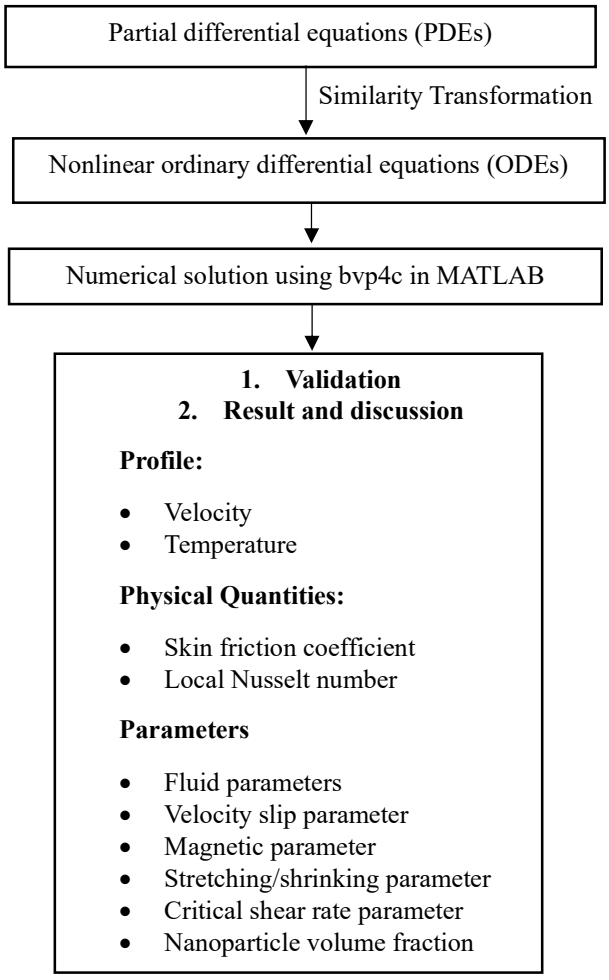

Figure 4. Methodology Framework

3.2 Mathematical Formulation

In this study, a steady, two-dimensional and incompressible flow of non-Newtonian Eyring-Powell ternary nanofluid over the stretching/shrinking sheet that aligns with the x-axis and plane $y = 0$ of the cartesian coordinate system were considered, as depicted in Figure 5. The sheet is being stretched/shrinked with a linear velocity, $u_w = ax$ where a is a constant. T_∞ is the ambient temperature, T_w as the temperature at the wall, B is the magnetic field and slip velocity is presence along the surface. In this work, the ternary nanofluid used is engine oil as the base fluid and aluminium alloys (AA7072 and AA7075) and cobalt ferrite ($CoFe_2O_4$) nanoparticles.

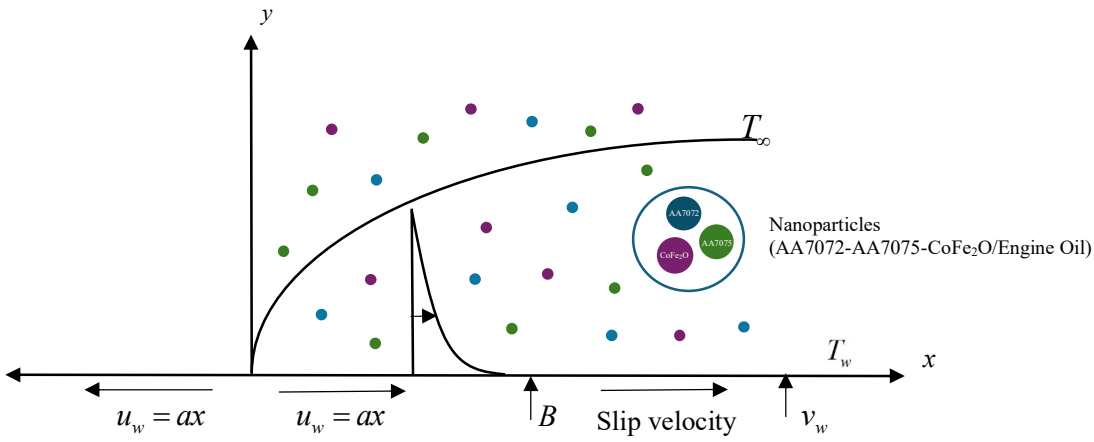

Figure 5: Sketch of the flow problem

Eyring-Powell model will be used where it is derived from the theory of rate processes for the purpose of explaining the shear of non-Newtonian flow. The equation to show the shear tensor, τ_w, in an Eyring-Powell model is given by Hayat et al. (2012)

$$\tau_w = \mu \frac{\partial u_i}{\partial x_j} + \frac{1}{\beta} \sinh^{-1}\left(\frac{1}{E}\frac{\partial u_i}{\partial x_j}\right) \tag{1}$$

where μ is the dynamic viscosity while $\beta = \beta_0 x^{-1}$ and $E = E_0 x$ are the Eyring-Powell model's fluid parameters. The second order function of $\sinh^{-1}$ approximation is used as

$$\sinh^{-1}\left(\frac{1}{E}\frac{\partial u_i}{\partial x_j}\right) \cong \frac{1}{E}\frac{\partial u_i}{\partial x_j} - \frac{1}{6}\left(\frac{1}{E}\frac{\partial u_i}{\partial x_j}\right)^3, \left|\frac{1}{E}\frac{\partial u_i}{\partial x_j}\right| << 1 \tag{2}$$

The boundary layer approximation can simplify the equation of continuity, momentum (Agrawal & Kaswan, 2021) and energy equation (Oke & Mutuku, 2021) for an incompressible fluid that obeys Eyring-Powell. The equations are as follows:

$$\frac{\partial u}{\partial x}+\frac{\partial v}{\partial y}=0\,, \tag{3}$$

$$u\frac{\partial u}{\partial x}+v\frac{\partial u}{\partial y}=\left(\frac{\mu_{thnf}}{\rho_{thnf}}+\frac{1}{\rho_{thnf}\beta E}\right)\frac{\partial^2 u}{\partial y^2}-\frac{1}{2\rho_{thnf}\beta E^3}\left(\frac{\partial u}{\partial y}\right)^2\frac{\partial^2 u}{\partial y^2}-\frac{\sigma_{thnf}B^2u}{\rho_{thnf}}\,, \tag{4}$$

$$u\frac{\partial T}{\partial x}+v\frac{\partial T}{\partial y}=\frac{k}{\left(\rho C_P\right)_{thnf}}\frac{\partial^2 T}{\partial y^2} \tag{5}$$

where u and v along the x and y-directions are velocity components, ρ is the fluid density, μ is the dynamic viscosity, T as temperature, and σ represents the electrical conductivity of the fluid. k represents the thermal conductivity of the liquid and C_p denotes the specific heat. The subscript $thnf$ refers to ternary nanofluid.

The boundary condition applicable are (Abbas et al., 2019)

$$\begin{aligned} u=\lambda u_w+u_t=\lambda ax+\gamma^*\left(1-\xi^*\frac{\partial u}{\partial y}\right)^{-\frac{1}{2}}\frac{\partial u}{\partial y}, \quad v=v_w=\sqrt{av_f}\,S\,, \qquad & T=T_w\text{, at } y=0 \\ u\to 0 \qquad\qquad\qquad\qquad\qquad\qquad & T\to T_\infty \text{ as } y\to\infty \end{aligned} \tag{6}$$

Here γ^* denotes the Navier slip length, $\xi^*=n^*x^{-1}$ represents the reciprocal of shear rate where n^* is a constant, λ is the stretching/shrinking parameter, S is the suction parameter, and u_t is the tangential velocity.

Ternary hybrid nanofluid's thermophysical properties (Hussain et al., 2024) are provided as follows:

$$\mu_{thnf}=\frac{\mu_{bf}}{\left(1-\phi\right)^{2.5}}\ \text{where}\ \phi=\phi_1+\phi_2+\phi_3 \tag{7}$$

$$\rho_{thnf} = (1-\phi_2)[(1-\phi_2)\{(1-\phi_3)\rho_{bf} + \phi_3\rho_3\} + \phi_2\rho_2] + \phi_1\rho_1 \tag{8}$$

$$k_{thnf} = k_{hnf}\left[\frac{k_1 + 2k_{hnf} - 2\phi_1\left(k_{hnf} - k_1\right)}{k_1 + 2k_{hnf} + \phi_1(k_{hnf} - k_1)}\right] \text{ where}$$

$$k_{hnf} = k_{nf}\left[\frac{2k_{nf} + k_2 - 2\phi_2(k_{nf} - k_2)}{k_2 + 2k_{nf} + \phi_2(k_{nf} - k_2)}\right] \text{ and } k_{nf} = k_{bf}\left[\frac{2k_{bf} + k_3 - 2\phi_3(k_{bf} - k_3)}{k_3 + 2k_{bf} + \phi_3(k_{bf} - k_3)}\right] \tag{9}$$

$$\sigma_{thnf} = \sigma_{hnf}\left[\frac{\sigma_1\left(1+2\phi_1\right) + \sigma_{hnf}(1-2\phi_1)\phi_1 + \sigma_2\phi_2}{\sigma_1\left(1-\phi_1\right) + \sigma_{hnf}(1+\phi_1)}\right] \text{ where}$$

$$\sigma_{hnf} = \sigma_{nf}\left[\frac{\sigma_2\left(1+2\phi_2\right) + \sigma_{nf}(1-2\phi_2)}{\sigma_2\left(1-\phi_2\right) + \sigma_{nf}(1+\phi_2)}\right] \text{ and } \sigma_{nf} = \sigma_{bf}\left[\frac{\sigma_3\left(1+2\phi_3\right) + \sigma_{bf}(1-2\phi_3)}{\sigma_3\left(1-\phi_3\right) + \sigma_{bf}(1+\phi_3)}\right] \tag{10}$$

$$\left(\rho C_p\right)_{thnf} = \left(\rho C_p\right)_1\phi_1 + \left(1-\phi_1\right)\left[(1-\phi_2)\left\{\left(1-\phi_3\right)\left(\rho C_p\right)_{bf} + \phi_3\left(\rho C_p\right)_3\right\} + \phi_2\left(\rho C_p\right)_2\right] \tag{11}$$

where ϕ is nanoparticle volume fraction, ϕ_1 is volume fraction of nanoparticle AA7072, ϕ_2 is volume fraction of nanoparticle AA7075, ϕ_3 is the volume fraction of nanoparticle $CoFe_2O_4$, $\left(\rho C_p\right)$ is heat capacity and subscript *bf* denotes the base fluid while *hnf* represents hybrid nanofluid.

Table 1 shows the thermophysical properties of the base fluid engine oil with its nanoparticles which are aluminium alloys (AA7072 and AA7075) and cobalt ferrite ($CoFe_2O_4$).

Table 1. Thermophysical Properties of Engine Oil, Aluminium Alloys (AA7072, AA7075), and Cobalt Ferrite ($CoFe_2O_4$) (Adnan et al., 2021; Karthikeyan et al., 2024; Khan et al., 2023)

Physical properties	Engine oil	AA7072	AA7075	$CoFe_2O_4$
C_p (J/kg K)	1910	893	960	700
ρ (kg/m^3)	884	2720	2810	4907
k (W/mK)	0.144	222	173	3.7
σ (S/m)	2.1×10^{-12}	34.83×10^{6}	26.77×10^{6}	5.51×10^{9}

Then, the fluid exerts force onto the surface which also referred to as a local skin friction coefficient, C_f , given as:

$$C_f = \frac{\tau_w}{\rho_{thnf} u_w^{\,2}}, \tag{12}$$

$$\tau_w = \left[\left(\mu_{thnf} + \frac{1}{\beta E} \right) \frac{\partial u}{\partial y} - \frac{1}{6\beta E^3} \left(\frac{\partial u}{\partial y} \right)^3 \right]_{y=0}. \tag{13}$$

where τ_w is shear stress.

The equations for Nu_x, Nusselt number is

$$Nu_x = \frac{x q_w}{k_f (T_w - T_\infty)}, \tag{14}$$

$$q_w = -k_{thnf} \left(\frac{\partial T}{\partial y} \right)_{y=0}. \tag{15}$$

where q_w is heat flux

The similarity variables will be used to transform the partial differential equations into higher order non-linear ordinary differential equations (ODEs) by executing similarity transformation. The variables are defined as follows (Hayat et al., 2013):

$$u = axf'(\eta), \quad v = -\sqrt{a(v_f)} f(\eta), \quad \eta = \sqrt{\frac{a}{v_f}} y, \quad \theta(\eta) = \frac{T - T_\infty}{T_w - T_\infty} \tag{16}$$

where the η denotes the similarity variable, f and θ are dimensionless stream function and dimensionless temperature respectively, and v_f is kinematic viscosity while (') is the differentiation with the respect to η.

3.3 Transformation of continuity equation

Differentiating u with respect to x and v with the respect to y partially, we obtain:

$$\frac{\partial u}{\partial x} = af', \tag{17}$$

$$\frac{\partial v}{\partial y} = -\sqrt{av_f}\left(\sqrt{\frac{a}{v_f}}\right)f' = -af'. \tag{18}$$

From continuity equation (3), substitute equations (17) and (18) :

$$af' - af' = 0. \tag{19}$$

Therefore, the continuity equation is satisfied.

3.4 Transformation of momentum equation

The u is derived to second order with respect to y as below

$$\frac{\partial u}{\partial y} = ax\sqrt{\frac{a}{v_f}}f'', \tag{20}$$

$$\frac{\partial^2 u}{\partial y^2} = \frac{a^2}{v_f}xf'''. \tag{21}$$

The equation of (16), (17), (20) and (21) are substituted into the momentum equation (4)

$$a^2xf'^2-a^2xff''=\left(\frac{\mu_{thnf}}{\rho_{thnf}}+\frac{1}{\rho_{thnf}\beta_0x^{-1}E_0x}\right)\left(\frac{a^2}{v_f}xf'''\right)$$
$$-\frac{1}{2\rho_{thnf}\beta_0x^{-1}E_0{}^3x^3}\left(ax\sqrt{\frac{a}{v_f}}f''\right)^2\left(\frac{a^2}{v_f}xf'''\right)-\frac{\sigma_{thnf}B^2}{\rho_{thnf}}(axf'),$$

$$a^2xf'^2-a^2xff''=\left(\frac{\mu_{thnf}}{\rho_{thnf}}+\frac{1}{\rho_{thnf}\beta_0x^{-1}E_0x}\right)\left(\frac{a^2}{v_f}xf'''\right)$$
$$-\frac{1}{2\rho_{thnf}\beta_0x^{-1}E_0{}^3x^3}\left(\frac{a^3}{v_f}x^2f''^2\right)\left(\frac{a^2}{v_f}xf'''\right)-\frac{\sigma_{thnf}B^2}{\rho_{thnf}}(axf'). \quad (23)$$

Factorisation by a^2x and rearranging equation (23) lead to

$$a^2x(f'^2-ff'')=a^2x[\left(\frac{\mu_{thnf}}{\rho_{thnf}}+\frac{1}{\rho_{thnf}\beta_0E_0}\right)\left(\frac{1}{v_f}f'''\right)$$
$$-\frac{1}{2\rho_{thnf}\beta_0E_0{}^3}\left(\frac{a^3}{v_f}f''^2\right)\left(\frac{1}{v_f}f'''\right)-\frac{\sigma_{thnf}B^2}{a\rho_{thnf}}(f')],$$

$$f'^2-ff''=\left(\frac{\mu_{thnf}}{\rho_{thnf}}+\frac{1}{\rho_{thnf}\beta_0E_0}\right)\left(\frac{f'''}{v_f}\right)-\frac{1}{2\rho_{thnf}\beta_0E_0{}^3}\left(\frac{a^3}{v_f{}^2}f''^2f'''\right)-\frac{\sigma_{thnf}B^2}{a\rho_{thnf}}f',$$

$$\left(\frac{\mu_{thnf}}{\rho_{thnf}}+\frac{1}{\rho_{thnf}\beta_0E_0}\right)\left(\frac{f'''}{v_f}\right)-\frac{1}{2\rho_{thnf}\beta_0E_0{}^3}\left(\frac{a^3}{v_f{}^2}f''^2f'''\right)-\frac{\sigma_{thnf}B^2}{a\rho_{thnf}}f'-(f'^2-ff'')=0. \quad (24)$$

Where $v_f=\frac{\mu_f}{\rho_f}$ is substituted into equation (24) and the equation is then multiplied by $\frac{\rho_{thnf}}{\rho_f}$ to gives

$$\left(\frac{\mu_{thnf}}{\rho_{thnf}}+\frac{1}{\rho_{thnf}\beta_0E_0}\right)\left(\frac{f'''}{\mu_f/\rho_f}\right)-\frac{1}{2\rho_{thnf}\beta_0E_0{}^3}\left(\frac{a^3}{(\mu_f/\rho_f)v_f}f''^2f'''\right)$$
$$-\frac{\sigma_{thnf}B^2}{a\rho_{thnf}}f'-(f'^2-ff'')=0, \quad (25)$$

Rearrange the equation (25)

$$\frac{\mu_{thnf}}{\mu_f} f''' + \frac{1}{\mu_f \beta_0 E_0} f''' - \frac{a^3}{2\mu_f \beta_0 E_0^{\,3} v_f}\left(f''^2 f'''\right) - \frac{\sigma_{thnf} B^2}{a\rho_{thnf}}\left(\frac{\rho_{thnf}}{\rho_f}\right) f' - \frac{\rho_{thnf}}{\rho_f}\left(f'^2 + ff''\right) = 0,$$

$$\left(\frac{\mu_{thnf}}{\mu_f} + \beta_1 - E_1 \beta_1 f''^2\right)\left(f'''\right) - \frac{\sigma_{thnf} B^2}{a\rho_{thnf}}\left(\frac{\rho_{thnf}}{\rho_f}\right) f' - \frac{\rho_{thnf}}{\rho_f}(f'^2 - ff'') = 0. \quad (26)$$

Where $\beta_1 = \frac{1}{\mu_f \beta_0 E_0}$ and $E_1 = \frac{a^3}{2E_0^{\,2} v_f}$ are the Eyring-Powell fluid parameters.

Rearrange equation (26)

$$\left(\frac{\mu_{thnf}}{\mu_f} + \beta_1 - E_1 \beta_1 f''^2\right)\left(f'''\right) - \frac{\sigma_{thnf} B^2}{a\rho_f}\left(\frac{\sigma_f}{\sigma_f}\right) f' - \frac{\rho_{thnf}}{\rho_f}(f'^2 - ff'') = 0,$$

$$\left(\frac{\mu_{thnf}}{\mu_f} + \beta_1 - E_1 \beta_1 f''^2\right)\left(f'''\right) - \frac{\sigma_{thnf}}{\sigma_f} M f' - \frac{\rho_{thnf}}{\rho_f}(f'^2 - ff'') = 0 \quad (27)$$

Where $M = \frac{\sigma_f}{a\rho_f} B^2$ is the magnetic parameter.

3.5 Transformation of energy equation

In transforming energy equation (5), we rearrange and differentiate the equation of temperature with the respect of x and y respectively

$$T = \left(T_w - T_\infty\right)\theta\left(\eta\right) + T_\infty, \quad (28)$$

$$\frac{\partial T}{\partial x} = 0, \quad (29)$$

$$\frac{\partial T}{\partial y} = \left(T_w - T_\infty\right)\sqrt{\frac{a}{v_f}}\theta', \quad (30)$$

$$\frac{\partial^2 T}{\partial y^2} = \left(T_w - T_\infty\right)\frac{a}{v_f}\theta''. \quad (31)$$

Substitution of equations (16), (28) – (31) into equation (5) gives

$$-\sqrt{av_f}\,f\left(T_w-T_\infty\right)\sqrt{\frac{a}{v_f}}\theta'=\frac{k_{thnf}}{\left(\rho C_p\right)_{thnf}}\left(T_w-T_\infty\right)\frac{a}{v_f}\theta''. \tag{32}$$

By dividing equation (32) by $a\left(T_w-T_\infty\right)$ and rearranging the terms, we have

$$-af\left(T_w-T_\infty\right)\theta'=\frac{k_{thnf}}{\left(\rho C_p\right)_{thnf}}\left(T_w-T_\infty\right)\frac{a}{v_f}\theta'',$$

$$-f\theta'=\frac{k_{thnf}}{\left(\rho C_p\right)_{thnf}}\frac{1}{v_f}\theta'',$$

$$\frac{k_{thnf}}{\left(\rho C_p\right)_{thnf}}\frac{1}{v_f}\theta''+f\theta'=0. \tag{33}$$

where $\Pr=\dfrac{\mu_f\left(C_p\right)_f}{k_f}$. Rearranging equation (33) gives

$$\frac{k_{thnf}}{\left(\rho C_p\right)_{thnf}}\frac{\rho_f}{\mu_f}\theta''+f\theta'=0,$$

$$\frac{k_{thnf}}{\left(\rho C_p\right)_{thnf}}\frac{\rho_f}{\mu_f}\frac{k_f}{k_f}\frac{\left(C_p\right)_f}{\left(C_p\right)_f}\theta''+f\theta'=0,$$

$$\frac{k_{thnf}/k_f}{\left(\rho C_p\right)_{thnf}/\left(\rho C_p\right)_f}\left(\frac{k_f}{\mu_f\left(C_p\right)_f}\right)\theta''+f\theta'=0,$$

$$\frac{k_{thnf}/k_f}{\left(\rho C_p\right)_{thnf}/\left(\rho C_p\right)_f}\left(\frac{1}{\Pr}\right)\theta''+f\theta'=0 \tag{34}$$

3.6 Transformation of boundary condition equation

When $y=0$,

$$\eta = \sqrt{\frac{a}{v_f}}(0),$$
$$\eta = 0. \tag{35}$$

- $v = \sqrt{av_f}S$ at $y = 0$

$$v = v_w,$$
$$\sqrt{av_f}f(0) = \sqrt{av_f}S,$$
$$f(0) = S.$$

- $T = T_w$ at $y = 0$

$$T = (T_w - T_\infty)\theta(\eta) + T_\infty,$$
$$T_w = (T_w - T_\infty)\theta(0) + T_\infty,$$
$$\theta(0) = \frac{T_w - T_\infty}{T_w - T_\infty},$$
$$\theta(0) = 1.$$

- $u = u_w\lambda + u_t$ at $y = 0$

$$axf'(0) = \lambda ax + \gamma^*\left(1 - n^* x^{-1}\left(ax\sqrt{\frac{a}{v_f}}f''(0)\right)\right)^{-\frac{1}{2}}\left(ax\sqrt{\frac{a}{v_f}}f''(0)\right),$$
$$axf'(0) = \lambda ax + \gamma^*\left(1 - n^*\left(a\sqrt{\frac{a}{v_f}}f''(0)\right)\right)^{-\frac{1}{2}}\left(ax\sqrt{\frac{a}{v_f}}f''(0)\right). \tag{36}$$

Equation (36) is then simplified

$$f'(0) = \lambda + \gamma^*\left(\sqrt{\frac{a}{v_f}}\right)\left(1 - n^*\left(a\sqrt{\frac{a}{v_f}}f''(0)\right)\right)^{-\frac{1}{2}}(f''(0)),$$
$$f'(0) = \lambda + L_1(1 - L_2 f''(0))^{-\frac{1}{2}}(f''(0)).$$

where L_1 and L_2 are velocity slip parameter and critical shear rate respectively and are expressed as

$$L_1 = \sqrt{\frac{a}{v_f}}\gamma^*,\ L_2 = a\sqrt{\frac{a}{v_f}}n^*.$$

The second boundary condition which is $u \to 0$, $T \to T_\infty$ as $y \to \infty$ is applied to the similarity variables (16),

As $y \to \infty$,

$$\eta \to \sqrt{\frac{a}{v_f}}(\infty) = \infty,$$
$$\eta \to \infty$$

- $u \to 0$ as $y \to \infty$

$$\begin{aligned} u &\to 0, \\ axf'(\eta) &\to 0, \\ f'(\eta) &\to 0. \end{aligned} \tag{37}$$

- $T \to T_\infty$ as $y \to \infty$

$$\begin{aligned} (T_w - T_\infty)\theta(\eta) + T_\infty &\to T_\infty, \\ (T_w - T_\infty)\theta(\eta) &\to T_\infty - T_\infty, \\ \theta(\eta) &\to 0, \end{aligned}$$

The boundary condition (6) becomes

$$\begin{gathered} f(0) = S, f'(0) = \lambda + L_1\left(1 - L_2 f''(0)\right)^{-\frac{1}{2}}\left(f''(0)\right), \theta(0) = 1 \\ f'(\eta) \to 0, \theta(\eta) \to 0 \text{ as } \eta \to \infty. \end{gathered} \tag{38}$$

3.7 Transformation of local skin friction

Substitute equation (20) when $y = 0$ into equation (13), we have

$$\tau_w = \left(\mu_{thnf} + \frac{1}{\beta E}\right)\left(ax\sqrt{\frac{a}{v_f}}f''(0)\right) - \frac{1}{6\beta E^3}\left(ax\sqrt{\frac{a}{v_f}}f''(0)\right)^3. \tag{39}$$

Substitution of equation (39) into (12) gives

$$C_f = \frac{\left(\mu_{thnf} + \frac{1}{\beta E}\right)\left(ax\sqrt{\frac{a}{v_f}}f''(0)\right) - \frac{1}{6\beta E^3}\left(ax\sqrt{\frac{a}{v_f}}f''(0)\right)^3}{\rho_f (ax)^2}. \tag{40}$$

Factorising the term $\sqrt{\frac{a}{v_f}}$ from equation (40),

$$C_f = \frac{\sqrt{\frac{a}{v_f}}\left[\left(\mu_{thnf} + \frac{1}{\beta E}\right)(f''(0)) - \frac{1}{6\beta E^3}(ax)^2\frac{a}{v_f}(f''(0))^3\right]}{\rho_f ax}. \tag{41}$$

Rearranging equation (41),

$$C_f = \sqrt{\frac{1}{av_f}}\frac{1}{\rho_f x}\left[\left(\mu_{thnf} + \frac{1}{\beta E}\right)(f''(0)) - \frac{1}{6\beta E^3}(ax)^2\frac{a}{v_f}(f''(0))^3\right],$$

$$C_f = \sqrt{\frac{v_f}{a}}\frac{\rho_f}{\mu_f}\frac{1}{\rho_f x}\left[\left(\mu_{thnf} + \frac{1}{\beta E}\right)(f''(0)) - \frac{1}{6\beta E^3}(ax)^2\frac{a}{v_f}(f''(0))^3\right],$$

$$C_f = \sqrt{\frac{v_f}{a}}\frac{1}{x}\left[\left(\frac{\mu_{thnf}}{\mu_f} + \frac{1}{\beta_0 x^{-1}E_0 x\mu_f}\right)(f''(0)) - \frac{1}{6\beta_0 x^{-1}E_0{}^3 x^3\mu_f}(ax)^2\frac{a}{v_f}(f''(0))^3\right]. \tag{42}$$

Equation (42) is then rearranged

$$C_f = \mathrm{Re}_x^{-\frac{1}{2}}\left[\left(\frac{\mu_{thnf}}{\mu_f} + \frac{1}{\beta_0 x^{-1}E_0 x\mu_f}\right)(f''(0)) - \frac{1}{6\beta_0 E_0{}^3\mu_f}\frac{a^3}{v_f}(f''(0))^3\right] \tag{43}$$

where $\mathrm{Re}_x = \frac{u_w x}{v_f}$ is the Reynold number. By rearranging equation (43), we obtain

$$\mathrm{Re}_x^{\frac{1}{2}} C_f = \left(\frac{\mu_{thnf}}{\mu_f} + \frac{1}{\beta_0 x^{-1} E_0 x \mu_f} \right) \left(f''(0) \right) - \frac{1}{6\beta_0 E_0^{\,3} \mu_f} \frac{a^3}{\nu_f} (f''(0))^3,$$

$$\mathrm{Re}_x^{\frac{1}{2}} C_f = \left(\frac{\mu_{thnf}}{\mu_f} + \beta_1 \right) f''(0) - \frac{\beta_1 E_1}{3} \left(f''(0) \right)^3 . \tag{44}$$

3.7 Transformation of Nusselt number

Equation (30) when $y = 0$ is substituted into equation (15) to gives

$$q_w = -k_{thnf} \left(T_w - T_\infty \right) \left(\sqrt{\frac{a}{\nu_f}} \right) \theta'(0) . \tag{45}$$

Substituting equation (45) into equation (14) yields

$$Nu_x = \frac{x(-k_{thnf}) \left(T_w - T_\infty \right) \left(\sqrt{\frac{a}{\nu_f}} \right) \theta'(0)}{k_f \left(T_w - T_\infty \right)} . \tag{46}$$

Equation (46) is then simplified by cancelling out the common factor $T_w - T_\infty$ in the numerator and denominator,

$$Nu_x = \frac{-k_{thnf} x \left(\sqrt{\frac{a}{\nu_f}} \right) \theta'(0)}{k_f},$$

$$Nu_x = \frac{-k_{thnf} \, \mathrm{Re}_x^{\frac{1}{2}} \theta'(0)}{k_f},$$

$$\mathrm{Re}_x^{-\frac{1}{2}} Nu_x = \frac{-k_{thnf}}{k_f} \theta'(0). \tag{47}$$

3.8 Numerical Method

The set of the ODEs from equation (27) and (34) and the physical parameters, (44) and (47) were solved under the influence of boundary conditions using MATLAB's built-in solver, which is the bvp4c. New variables were introduced to convert the higher-order equations into the first-order equations.

$$\begin{aligned} &y(1) = f, \\ &y'(1) = y(2) = f', \\ &y'(2) = y(3) = f'' \end{aligned} \tag{48}$$

and

$$\begin{aligned} &y(4) = \theta, \\ &y'(4) = y(5) = \theta'. \end{aligned} \tag{49}$$

Equation (27) were rearranged and equations (48) was substituted to give

$$\begin{aligned} f''' &= \frac{\frac{\sigma_{thnf}}{\sigma_f} Mf' + \frac{\rho_{thnf}}{\rho_f}\left(f'^2 - ff''\right)}{\frac{\mu_{thnf}}{\mu_f} + \beta_1 - E_1\beta_1 f''^2}, \\ f''' &= \frac{\frac{\sigma_{thnf}}{\sigma_f} My(2) + \frac{\rho_{thnf}}{\rho_f}\left(y^2(2) - y(1)y(3)\right)}{\frac{\mu_{thnf}}{\mu_f} + \beta_1 - E_1\beta_1 y^2(2)}, \\ y'(3) &= \frac{A_2 My(2) + A_3\left(y^2(2) - y(1)y(3)\right)}{A_1 + \beta_1 - E_1\beta_1 y^2(2)} \end{aligned} \tag{50}$$

where $A_1 = \frac{\mu_{thnf}}{\mu_f}$, $A_2 = \frac{\sigma_{thnf}}{\sigma_f}$, and $A_3 = \frac{\rho_{thnf}}{\rho_f}$. Then, the rearrangement of equation (34) with θ'' as the subject and the substitution of equations (48) and (49) yields

$$\theta'' = -\frac{\left(\left(\rho C_p\right)_{thnf} \Big/ \left(\rho C_p\right)_f\right) \Pr f\theta'}{\left(k_{thnf} \Big/ k_f\right)},$$

$$\theta'' = -\frac{A_5 \Pr y(1) y(5)}{A_4} \tag{51}$$

with $A_4 = \frac{k_{thnf}}{k_f}$ and $A_5 = \frac{\left(\rho C_p\right)_{thnf}}{\left(\rho C_p\right)_f}$.

Then, the boundary conditions (35) and (38)-(37) were expressed in new terms as follows:

- $\eta = 0$

$$f(0) = S, f'(0) = \lambda + L_1\left(1 - L_2 f''(0)\right)^{-\frac{1}{2}}\left(f''(0)\right), \theta(0) = 1,$$

$$ya(1) = S,\ ya(2) = \lambda + L_1\left(1 - L_2 (ya(3)\right)^{-\frac{1}{2}}\left(ya(3)\right),\ ya(4) = 1. \tag{52}$$

- $\eta \to \infty$

$$f'(\infty) \to 0, \theta(\infty) \to 0,$$

$$yb(2) \to 0,\ yb(4) \to 0.$$

where *ya* indicates the values at initial boundary while *yb* indicates the values at the upper boundary for the system

The set of the ODEs were solved under the influence of boundary conditions using a solver under MATLAB which is the function bvp4c. The system was solved using ODE function, boundary condition function and initial guess (Shampine & Kierzenka, 2000). The code used is where 'odefun' is a function that represents the ODEs, 'bcfun'' is a function that specifies the boundary conditions, 'solinit' provides an initial guess for the solution and 'options' is the optional structure for the solver options such as error control.

sol = bvp4c(odefun, bcfun, solinit, options);

After the implementation of the code, the solution was stored in 'sol' structure. The MATLAB code is provided in the appendix for reference.

CHAPTER 4

RESULTS AND DISCUSSION

4.1 Validation of Results

The validation values of the system obtained when the values of the magnetic parameter ($M = 0$), slip parameter ($L_1 = 0$), critical shear rate ($L_2 = 0$), and the concentration of the nanoparticles ($\phi_1 = \phi_2 = \phi_3 = 0$) are absence which then compared with past results from several studies. This is done to ensure the accuracy of the method used. In Table 2, the comparison with Javed et al. (2013) of $f''(0)$ is made with the different values of the Eyring-Powell fluid parameter, Table 3, the result for heat transfer ($-\theta'(0)$) is compared with Salleh et al. (2010) when the Prandtl number varies, while Table 4 show the comparison for the shear rate($f''(0)$) for shrinking sheet ($\lambda = -1$) and several suction, S values. These comparisons show a close consistency between the present and past research.

Table 2. A Comparison of $f''(0)$ and $\mathrm{Re}_x^{1/2} C_f$ with Javed et al. (2013) when $\mathrm{Pr} = 30$, $\lambda = 1$, $M = S = L_1 = L_2 = \phi_1 = \phi_2 = \phi_3 = 0$

		Javed et al. (2013)		**Present result**	
E_1	β_1	$f''(0)$	$\mathrm{Re}_x^{1/2} C_f$	$f''(0)$	$\mathrm{Re}_x^{1/2} C_f$
0.0	0.0	-1	-1	-1	-1
	0.2	-0.9131	-1.0954	-0.9129	-1.0954
	0.4	-0.8452	-1.1832	-0.8452	-1.1832
	0.6	-0.7906	-1.2649	-0.7906	-1.2649
0.1	0.2	-0.9159	-1.0940	-0.9159	-1.0940
	0.4	-0.8493	-1.1808	-0.8493	-1.1808
	0.6	-0.7950	-1.2620	-0.7950	-1.2620
0.2	0.2	-0.9190	-1.0924	-0.9190	-1.0924
	0.4	-0.8536	-1.1784	-0.8536	-1.1784
	0.6	-0.7997	-1.2590	-0.7997	-1.2590
0.3	0.2	-0.9222	-1.0909	-0.9222	-1.0909
	0.4	-0.8580	-1.1776	-0.8580	-1.1760
	0.6	-0.8045	-1.2560	-0.8045	-1.2560

Table 3. Comparison values of $-\theta'(0)$ when $\lambda = 1, M = S = E_1 = \beta_1 = L_1 = L_2 = \phi_1 = \phi_2 = \phi_3 = 0$ with Salleh et al. (2010) for different Pr

	Salleh et al. (2010)	**Present result**
Pr	$-\theta'(0)$	
0.72	0.46317	0.46316
1	0.58198	0.58198
3	1.16522	1.16526
5	1.56806	1.56805
7	1.89548	1.89540
10	2.30821	2.30800
100	7.76249	7.76565

Table 4. Comparison value of $f''(0)$ with Roşca & Pop (2013) when $\lambda = -1$ (shrinking sheet) for several values of S

	Roşca & Pop (2013)	**Present result**
S	$f''(0)$	
2.0	1.0106	1.0000
2.5	2.0000	2.0000
3.0	2.6180	2.6180

In the present study, the effects of magnetic (M), velocity slip (L_1), critical shear rate parameters (L_2), and the concentration of nanoparticles (ϕ_1, ϕ_2, ϕ_3) on the local skin friction, local Nusselt number, velocity profile and temperature profile were obtained and discussed. The default value used are $S = 2.5$ and $\text{Pr} = 30$ for engine oil-based hybrid nanofluids were used as recommended by Yahya et al. (2021) to achieve better accuracy.

4.2 The Effects of Magnetic Parameter on Velocity Profile and Temperature Profile, Local Skin Friction Coefficient, and Nusselt Number

Figure 6 shows the impact of increasing magnetic parameter to the velocity profile, $f'(\eta)$, along the shrinking sheet ($\lambda = -1.5$) for the default value of $\phi_1 = \phi_2 = \phi_3 = 0.1, \beta_1 = L_1 = L_2 = 0.5,$ and $E_1 = 0.8$. As the value of the magnetic parameter increases ($M = 0, 0.1, 0.2$), the velocity of the fluid also increases for the first solution in contrast of the second solution where the fluid velocity decreases. Then, Figure 7 depicts the influence of different values of magnetic parameter on the temperature profile where the rise

of magnetic parameter decreases for the first solution the temperature of the fluid while the second solution is increasing. The increase in the fluid velocity due to the presence of Lorentz force which enhances the velocity of the fluid, hence increasing the heat transfer between the surface and the fluid, leads to a lower temperature.

Meanwhile in Figure 8 and Figure 9, the effect of the magnetic parameter, M, to local skin friction coefficient, $C_f \operatorname{Re}_x^{1/2}$ and Nusselt number, $Nu \operatorname{Re}_x^{-1/2}$ are displayed respectively. It is revealed that both the local skin friction coefficient and Nusselt number increases with the increase in magnetic parameter. Since the magnetic field increases the velocity of the fluid, the heat transfers ability becomes better, hence higher Nusselt number for higher value of magnetic parameter. From the figures, it can be observed that the solution exists only when the $\lambda \geq \lambda_c = -1.6446$ for $M = 0$. When the value of the magnetic parameter increases, the range for the λ also increases such that when $M = 0.1$ ($\lambda \geq \lambda_c = -1.9694$) and $M = 0.2$ ($\lambda \geq \lambda_c = -2.5073$).

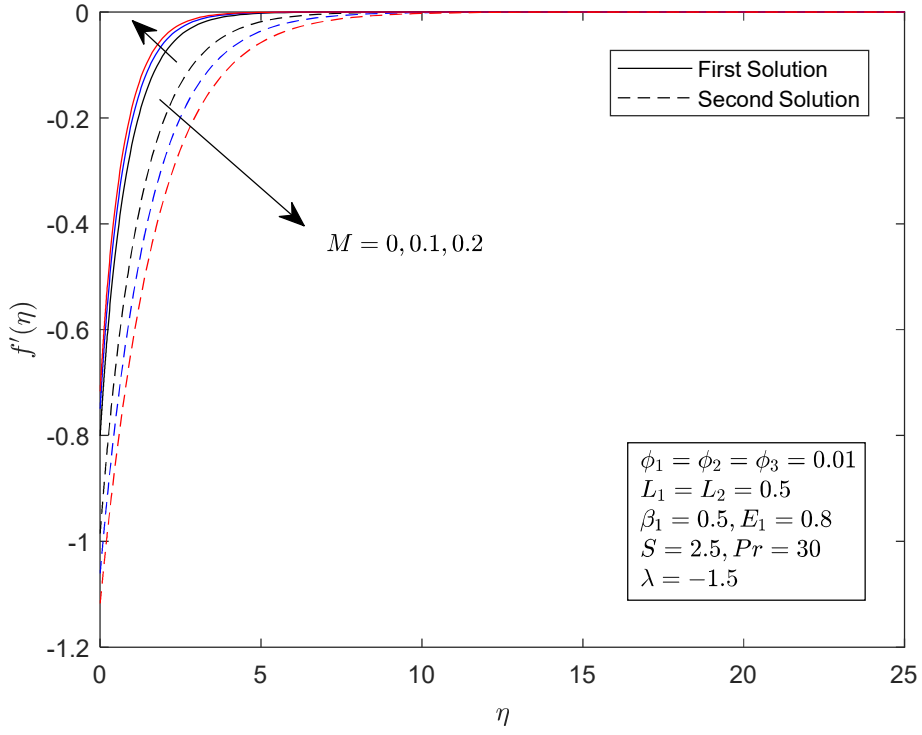

Figure 6. Influence of M on $f'(\eta)$.

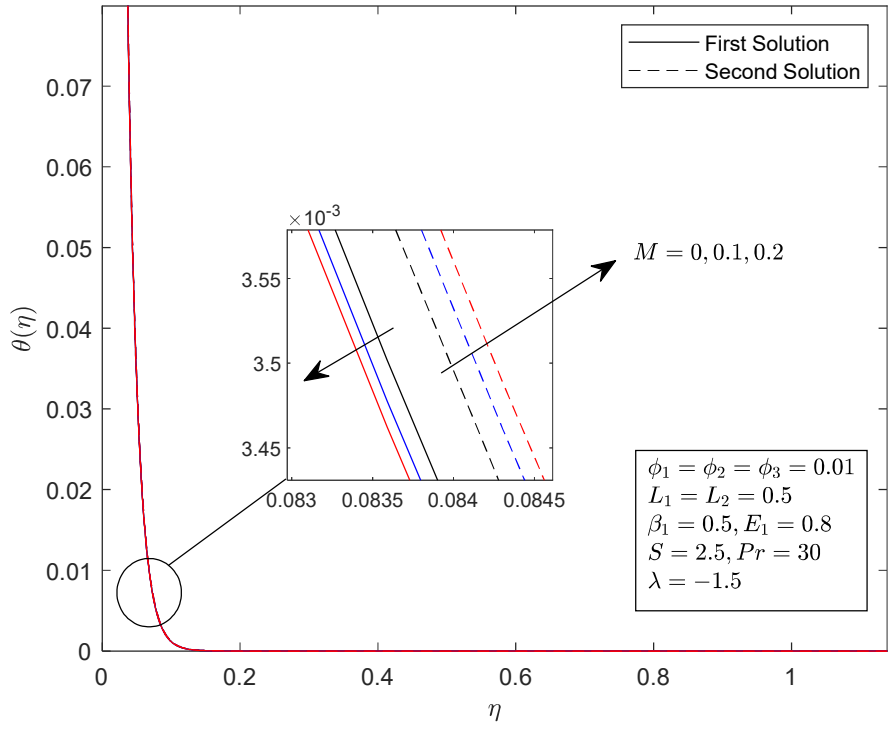

Figure 7. Influence of M on $\theta(\eta)$.

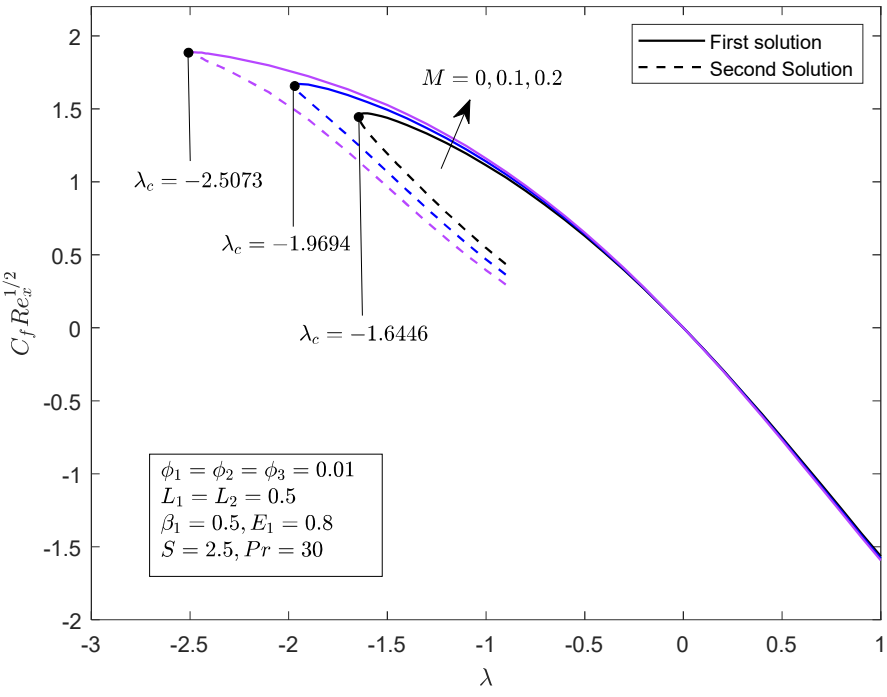

Figure 8. Local skin friction coefficient with various values of M.

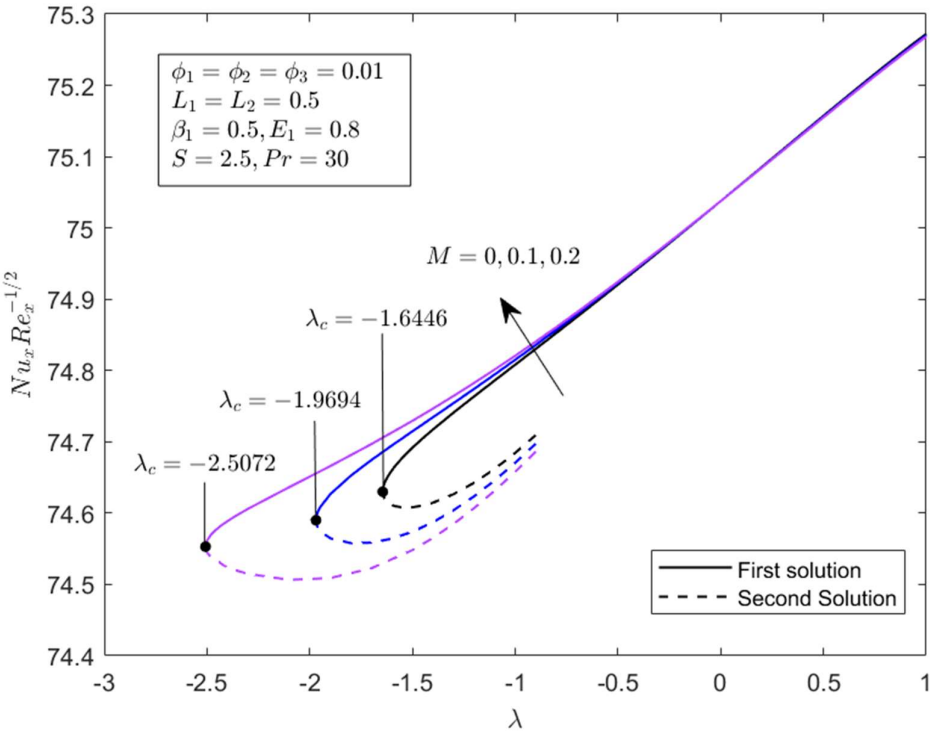

Figure 9. Local Nusselt number with various values of M .

4.3 Effects of Slip Velocity and Critical Shear Rate Parameters on Velocity Profile and Temperature Profile, Local Skin Friction Coefficient, and Nusselt Number

The impact of different values of velocity slip (L_1), critical shear rate parameters (L_2) with the default value sets to $\phi_1 = \phi_2 = \phi_3 = 0.1, M = 0.2, \beta_1 = 0.5,$ and $E_1 = 0.8$. on velocity profile, $f'(\eta)$ can be seen in Figure 10. The velocity of the ternary nanofluid fluid for the first solution increases with the increase in both slip velocity and critical shear rate parameters while the velocity profile for the second solution decreases. When velocity slip parameter is applied ($L_1 = 0.5$), there is less friction between the surface and the fluid due to the slip effect while the viscosity becomes weaker due to the presence of the critical shear rate parameter ($L_2 = 0.5, 0.6$) which resulting in higher fluid velocity. The graph for $L_1 = L_2 = 0.5$ and $L_1 = 0.5, L_2 = 0.6$ is closer than with the absence of velocity slip and critical shear rate parameters since there is only a slight difference in L_2 . Meanwhile, Figure 11

illustrates that as both slip velocity and critical shear rate parameters increases, the temperature profile, $\theta(\eta)$, decreases for first and second solution. When both of these parameters increase, the velocity of the fluid increases, enhancing the heat transfer between the fluid and the surface, hence, it has lower temperature profile.

Figure 12 shows the effect of slip velocity and critical shear rate parameters on the local skin friction coefficient, $C_f \operatorname{Re}_x^{1/2}$. When the value of the parameters increases, the local skin friction for the first solution decreases when $\lambda < 0$ while the second solution increases. From the figure, the local skin friction coefficient is slightly higher when there are no slip velocity and critical shear rate parameters being applied compared to when the values are $L_1 = L_2 = 0.5$ and $L_1 = 0.5, L_2 = 0.6$. On the other hand, Figure 13 reveals that the Nusselt number, $Nu \operatorname{Re}_x^{-1/2}$, for both solution rises with increasing slip velocity and critical shear rate parameters. It is observed dual solution exist during shrinking sheet until λ_c, before the separation boundary layer happens.

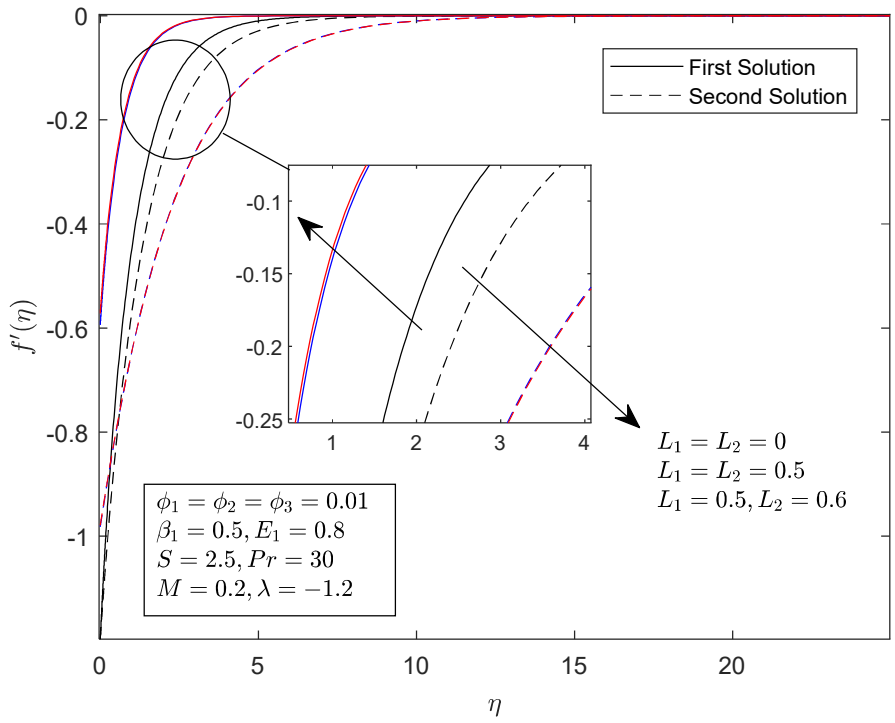

Figure 10. Influence of L_1 and L_2 on $f'(\eta)$.

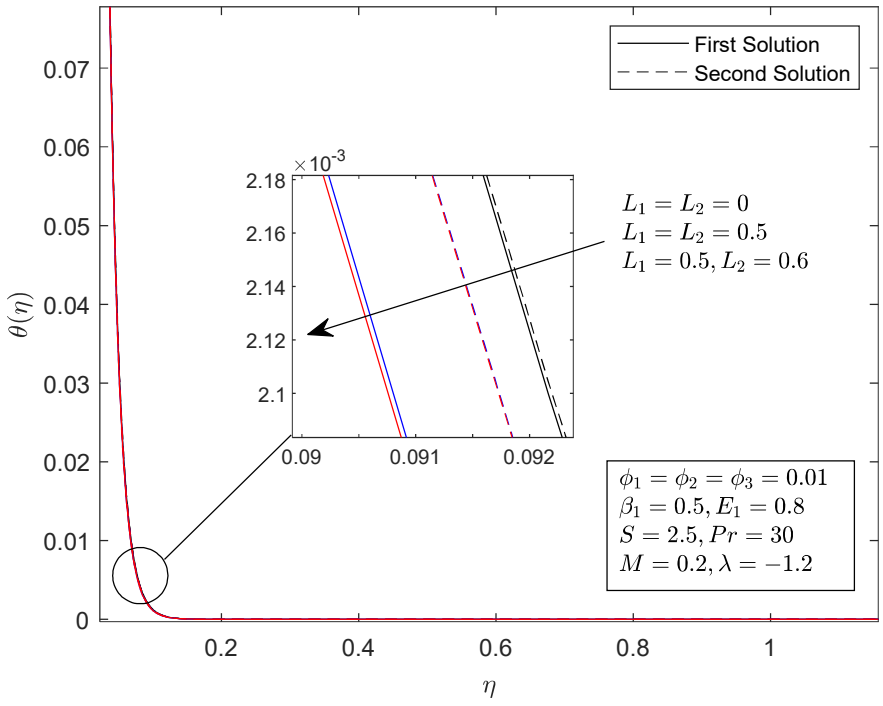

Figure 11. Influence of L_1 and L_2 on $\theta(\eta)$.

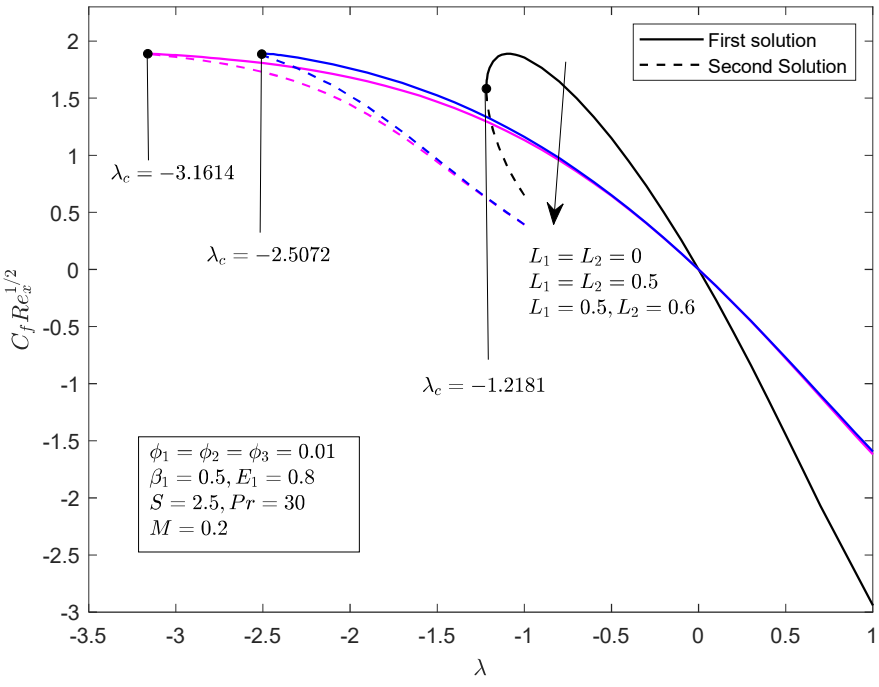

Figure 12. Local skin friction coefficient with various values of L_1 and L_2.

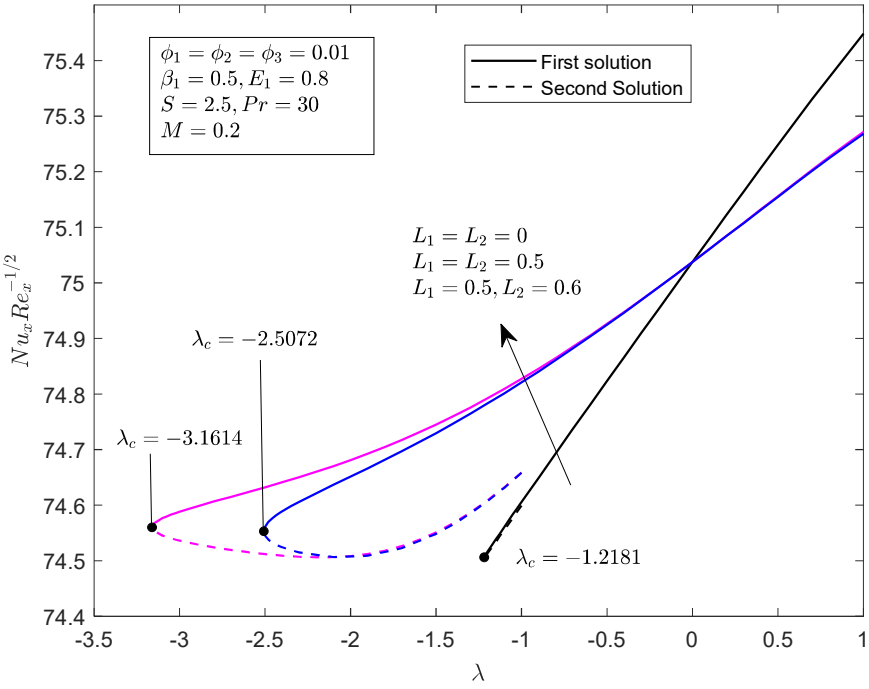

Figure 13. Local Nusselt number with various values of L_1 and L_2.

4.4 Effects of Volume Fraction of Nanoparticles on Velocity Profile and Temperature Profile, Local Skin Friction Coefficient, and Nusselt Number

The effects of different nanofluids were observed by setting the default value to $\phi_1 = 0.1, M = 0.2, \beta_1 = L_1 = L_2 = 0.5,$ and $E_1 = 0.8$. Figure 14 depicts the effects of nanofluid ($\phi_1 = 0.01, \phi_2 = \phi_3 = 0$), hybrid nanofluid ($\phi_1 = \phi_2 = 0.01, \phi_3 = 0$) and ternary nanofluid ($\phi_1 = \phi_2 = \phi_3 = 0.01$) to velocity profile where nanofluid has the highest fluid velocity, followed by hybrid and ternary nanofluid. This occurs due to the fact that the nanofluid's viscosity rises with an increase of the volume fraction of the nanoparticles which then causes resistance to the nanofluid. The increased resistance reduces the fluid velocity. The impacts of the volume fraction of nanoparticles on temperature are presented in Figure 15. The rise in the volume fraction of nanoparticles increases the temperature profile, $\theta(\eta)$. It is observed that the temperature profile is the lowest for the nanofluid, with hybrid nanofluid slightly higher and

ternary nanofluid has the highest temperature profile. This happens because of higher viscosity of the fluid promotes frictional heating which raises the temperature.

In Figure 16, it can be observed that the local skin friction, $C_f \operatorname{Re}_x^{1/2}$, increases when the volume fraction of the nanoparticles increases while Figure 17 shows that nanofluid have the highest Nusselt number, $Nu \operatorname{Re}_x^{-1/2}$, followed by ternary nanofluid and hybrid nanofluid. Both figures shows that the solutions exist for both stretching and shrinking sheet cases, while dual solution are observed only in shrinking region up to λ_c before the boundary layer become unstable. The solution exists when $\lambda \geq \lambda_c$ such that for the ternary nanofluid ($\lambda \geq \lambda_c = -2.5072$), followed by nanofluid ($\lambda \geq \lambda_c = -2.9509$) whereas hybrid nanofluid ($\lambda \geq \lambda_c = -3.1465$). Based on the Figure 16, ternary nanofluid has the highest skin friction due to its greater viscosity which enhance the resistance on the surface, while in Figure 17, Nanofluid exhibits the highest heat transfer performance due to its simpler composition.

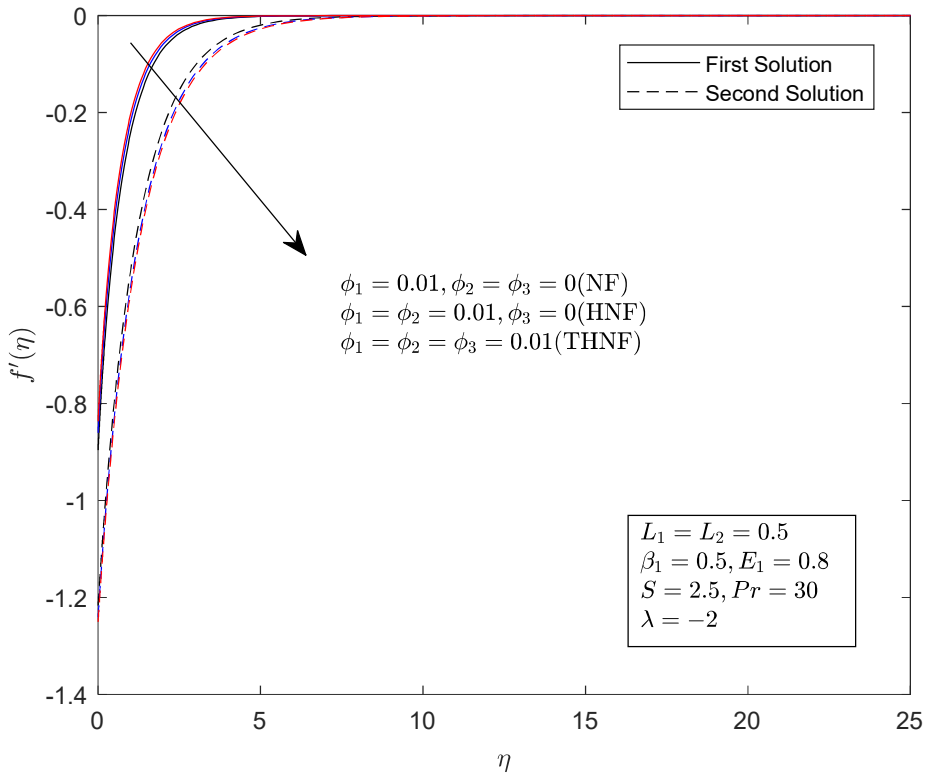

Figure 14. Influence of ϕ_1, ϕ_2 and ϕ_3 on $f'(\eta)$.

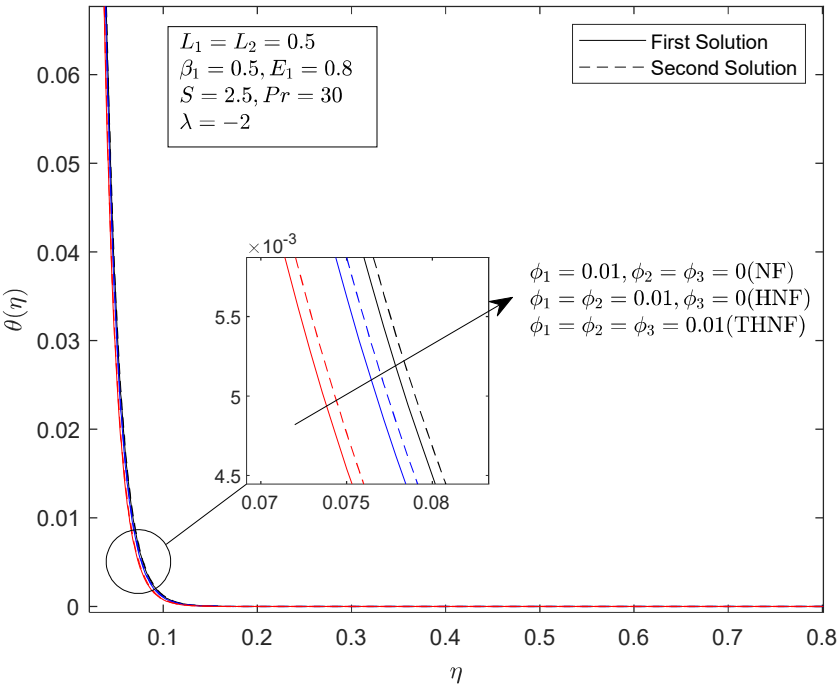

Figure 15. Influence of ϕ_1, ϕ_2 and ϕ_3 on $\theta(\eta)$.

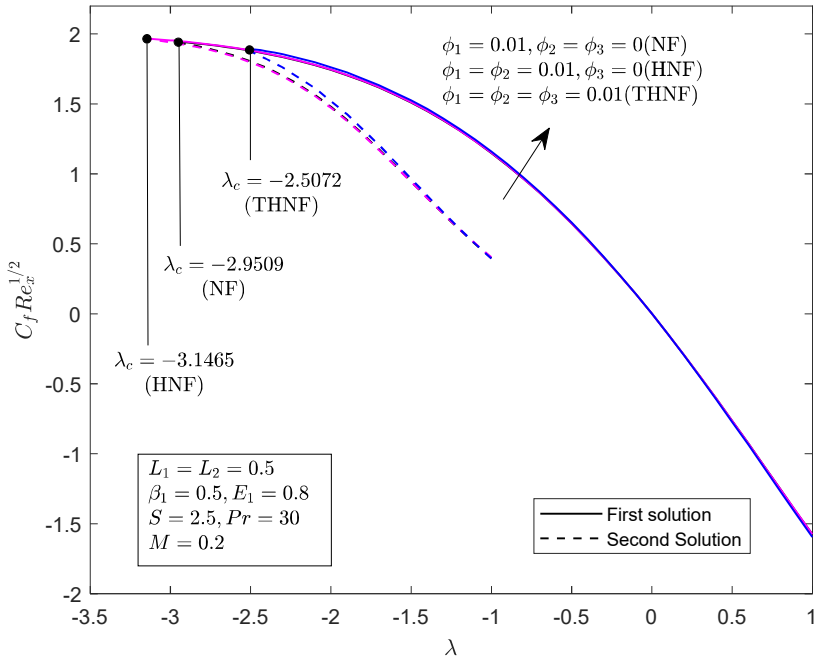

Figure 16. Local skin friction coefficient with various volume concentration of ϕ_1, ϕ_2 and ϕ_3.

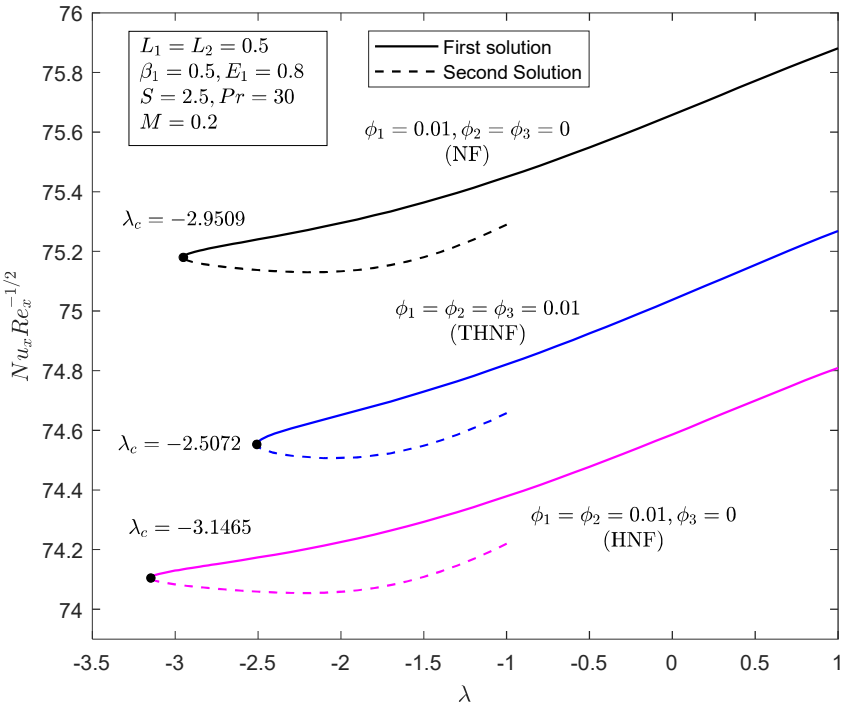

Figure 17. Local Nusselt number with various volume concentration of ϕ_1, ϕ_2 and ϕ_3.

CHAPTER 5

CONCLUSION AND RECOMMENDATION

5.1 Conclusion

In this study, Thomson and Troian slip on magnetohydrodynamic flow of Eyring-Powell ternary nanofluid past a shrinking/stretching sheet is considered. The boundary layer problem involves the continuity, momentum and energy equations, along with the boundary conditions, was transformed into a set of ordinary differential equations using the similarity variables. These equations were then solved using the MATLAB's built-in software, BVP4C solver. The impacts of various parameters which are volume fraction of nanoparticle, magnetic, slip velocity and critical shear rate parameters on local skin friction, Nusselt number, velocity and temperature profile were solved numerically, and the results were illustrated graphically. In conclusion, the results are:

- The velocity profile increases when there is an increase in magnetic, slip velocity, critical shear rate, and nanofluid has the highest velocity profile.
- The temperature of the fluid decreases when magnetic, slip velocity, critical shear rate parameters increase, and ternary nanofluid has the highest temperature profile.
- The skin friction rises with increasing in magnetic parameters but decreases with higher slip velocity, critical shear rate parameter while ternary nanofluid exhibit the highest skin friction.
- The Nusselt number is higher when there is an increase in magnetic, slip velocity, critical shear rate parameters, and nanofluid has the highest Nusselt number.
- In the graphs of local skin friction coefficient and Nusselt number, dual solution exists in the shrinking region until it reaches λ_c, where no solution exists beyond λ_c due to the separation of the boundary layer.

5.2 Recommendation

This presents study analyse the impact of magnetic parameter, volume fraction of nanoparticles and also in the presence of Thomson and Troian slip condition to the flow of the Eyring-Powell ternary nanofluid past both shrinking and stretching sheets. The nanoparticles chosen to be

studied in this research are aluminium alloys (AA7072 and AA7075) and cobalt ferrite ($CoFe_2O_4$) with engine oil as the base fluid. For future research, exploring different types of nanoparticles and how different types of nanoparticles can affect the boundary layer. Then, the study can also be extended by considering different parameters such as thermal radiation as it would be useful to capture a more complex and realistic scenarios.

REFERENCES

Abbas, Z., Sheikh, M., Hasnain, J., Ayaz, H., & Nadeem, A. (2019). Numerical aspects of Thomson and Troian boundary conditions in a Tiwari-Das nanofluid model with homogeneous-heterogeneous reactions. *Physica Scripta*, *94*(11). https://doi.org/10.1088/1402-4896/ab27f0

Adnan, Ullah Khan, S. I., Khan, U., Ahmed, N., Mohyud-Din, S. T., Khan, I., & Nisar, K. S. (2021). Thermal transport investigation in AA7072 and AA7075 aluminum alloys nanomaterials based radiative nanofluids by considering the multiple physical flow conditions. *Scientific Reports*, *11*(1). https://doi.org/10.1038/s41598-021-87900-w

Adun, H., Kavaz, D., & Dagbasi, M. (2021). Review of ternary hybrid nanofluid: Synthesis, stability, thermophysical properties, heat transfer applications, and environmental effects. *Journal of Cleaner Production*, *328*, 129525. https://doi.org/10.1016/j.jclepro.2021.129525

Agrawal, R., & Kaswan, P. (2021). MHD Eyring–Powell nanofluid past over an unsteady exponentially stretching surface with entropy generation and thermal radiation. *Heat Transfer*, *50*(5), 4669–4693. https://doi.org/10.1002/htj.22095

Ahmad, S., & Nadeem, S. (2020). Flow analysis by Cattaneo–Christov heat flux in the presence of Thomson and Troian slip condition. *Applied Nanoscience (Switzerland)*, *10*(12), 4673–4687. https://doi.org/10.1007/s13204-020-01267-4

Aich, W., Adnan, Sarfraz, G., Mahjoub Said, N., Bilal, M., Ahmed Elhag, A. F., & Hassan, A. M. (2023). Significance of radiated ternary nanofluid for thermal transport in stagnation point flow using thermal slip and dissipation function. *Case Studies in Thermal Engineering*, *51*. https://doi.org/10.1016/j.csite.2023.103631

Akaje, T. W., & Olajuwon, B. I. (2021). Impacts of Nonlinear Thermal Radiation on a Stagnation Point of an Aligned MHD Casson Nanofluid Flow with Thompson and Troian Slip Boundary Condition. *Journal of Advanced Research in Experimental Fluid Mechanics and Heat Transfer*, *6*(1), 1–15. http://www.akademiabaru.com/submit/index.php/arefmht

Akram, M., Shahzad, M. H., Ahammad, N. A., Gamaoun, F., Awan, A. U., Hamam, H., & Alroobaea, R. (2024). Rheology of Eyring–Powell hybrid nanofluid flow under the peristaltic effects through an elliptical conduit: Analytical investigation. *Results in Physics*, *59*. https://doi.org/10.1016/j.rinp.2024.107602

Aljabali, A., Abdul R. M. K., Khashi'ie, N. S., Iskandar, W., & Ariffin, N. A. N. (2023). Eyring-Powell Hybrid Nanofluid with Radiative Heat Flux: Case Over a Shrinking Sheet. *Journal of Advanced Research in Fluid Mechanics and Thermal Sciences*, *111*(1), 109–121. https://doi.org/10.37934/arfmts.111.1.109121

Aziz, A., Jamshed, W., Aziz, T., Bahaidarah, H. M. S., & Ur Rehman, K. (2020). Entropy analysis of Powell–Eyring hybrid nanofluid including effect of linear thermal radiation and viscous dissipation. *Journal of Thermal Analysis and Calorimetry*, *143*(2), 1331–1343. https://doi.org/10.1007/s10973-020-10210-2

Böhme, G. (2012). *Non-Newtonian Fluid Mechanics*. Elsevier.

Chalia, S., & Bharti, M. K. (2017). Design and Analysis of Vortex Generator and Dimple over an Airfoil Surface to Improve Aircraft Performance. *International Journal of Advanced Engineering Research and Applications*. www.ijaera.org

Chamsa-ard, W., Brundavanam, S., Fung, C., Fawcett, D., & Poinern, G. (2017). Nanofluid Types, Their Synthesis, Properties and Incorporation in Direct Solar Thermal Collectors: A Review. *Nanomaterials*, *7*(6), 131. https://doi.org/10.3390/nano7060131

Chhabra, R. P. (2010). *Non-Newtonian Fluids: An Introduction*.

De Vault, D. C., Libby, W. F., Segre, E., Halford, R. S., Seabourg, G. T., Siday, R. E., Mccreary, R. L., Valley, G. E., & Williams, E. J. (1939). Grinberg and Rossinow. In *Proc. Roy. Soc. A* (Vol. 55). https://royalsocietypublishing.org/

Dey, S., Mukhopadhyay, S., & Begum, M. (2022). Stefan flow of nanofluid and heat transport over a plate in company of Thompson and Troian slip and uniform shear flow. *Forces in Mechanics*, *9*, 100129. https://doi.org/10.1016/j.finmec.2022.100129

Dey, S., Mukhopadhyay, S., & Mandal, M. S. (2023). Influence of Thompson and Troian slip on the nanofluid flow past a permeable plate in porous medium. *Pramana - Journal of Physics*, *97*(2). https://doi.org/10.1007/s12043-023-02539-8

Fatunmbi, E. O., Ogunseye, H. A., & Sibanda, P. (2020). Magnetohydrodynamic micropolar fluid flow in a porous medium with multiple slip conditions. *International Communications in Heat and Mass Transfer*, *115*. https://doi.org/10.1016/j.icheatmasstransfer.2020.104577

Hayat, T., Iqbal, Z., Qasim, M., & Obaidat, S. (2012). Steady flow of an Eyring Powell fluid over a moving surface with convective boundary conditions. *International Journal of Heat and Mass Transfer*, *55*(7–8), 1817–1822. https://doi.org/10.1016/j.ijheatmasstransfer.2011.10.046

Hayat, T., Iqbal, Z., Qasim, M., & Alsaedi, A. (2013). Flow of an Eyring-Powell Fluid with Convective Boundary Conditions. *Journal of Mechanics*, *29*(2), 217–224. https://doi.org/10.1017/jmech.2012.135

Hayat, T., Ashraf, B., Shehzad, S. A., & Abouelmagd, E. (2015). Three-dimensional flow of Eyring Powell nanofluid over an exponentially stretching sheet. *International Journal of Numerical Methods for Heat & Fluid Flow*, *25*(3), 593–616. https://doi.org/10.1108/HFF-05-2014-0118

Hayat, T., & Nadeem, S. (2017). Heat transfer enhancement with Ag–CuO/water hybrid nanofluid. *Results in Physics*, *7*, 2317–2324. https://doi.org/10.1016/j.rinp.2017.06.034

Hussain, Z., Aljuaydi, F., Ayaz, M., & Islam, S. (2024). Enhancing thermal efficiency in MHD kerosene oil-based ternary hybrid nanofluid flow over a stretching sheet with convective boundary conditions. *Results in Engineering*, *22*, 102151. https://doi.org/10.1016/j.rineng.2024.102151

Ibrahim, W., & Tulu, A. (2019). Magnetohydrodynamic (MHD) Boundary Layer Flow Past a Wedge with Heat Transfer and Viscous Effects of Nanofluid Embedded in Porous Media. *Mathematical Problems in Engineering*, *2019*(1). https://doi.org/10.1155/2019/4507852

Ishak, A. (2011). *MHD Boundary Layer Flow Due to an Exponentially Stretching Sheet with Radiation Effect*.

Ishaq, M., Ali, G., Shah, Z., Islam, S., & Muhammad, S. (2018). Entropy Generation on Nanofluid Thin Film Flow of Eyring–Powell Fluid with Thermal Radiation and MHD Effect on an Unsteady Porous Stretching Sheet. *Entropy*, *20*(6), 412. https://doi.org/10.3390/e20060412

Javed, T., Ali, N., Abbas, Z., & Sajid, M. (2013). Flow of an eyring-powell non-newtonian fluid over a stretching sheet. *Chemical Engineering Communications*, *200*(3), 327–336. https://doi.org/10.1080/00986445.2012.703151

Karthikeyan, S., Ali, F., Loganathan, K., & Thamaraikannan, N. (2024). An implication of entropy generation in Maxwell fluid containing engine oil based ternary hybrid nanofluid over a riga plate. *Journal of Taibah University for Science*, *18*(1). https://doi.org/10.1080/16583655.2024.2387925

Khan, S. A., Hayat, T., & Alsaedi, A. (2023). KHA model comprising MoS4 and CoFe2O3 in engine oil invoking non-similar Darcy-Forchheimer flow with entropy and Cattaneo-Christov heat flux. *Nanoscale Advances*, *5*(22), 6135–6147. https://doi.org/10.1039/d3na00441d

Kumar, B., & Srinivas, S. (2020). Unsteady hydromagnetic flow of eyring-powell nanofluid over an inclined permeable stretching sheet with Joule Heating and thermal radiation. *Journal of Applied and Computational Mechanics*, *6*(2), 259–270. https://doi.org/10.22055/JACM.2019.29520.1608

Kundu, P. K., Cohen, I. M., & Dowling, D. R. (2016). *Fluid Mechanics (Sixth Edition)*. Elsevier.

Li, S., Puneeth, V., Saeed, A. M., Singhal, A., Al-Yarimi, F. A. M., Khan, M. I., & Eldin, S. M. (2023). Analysis of the Thomson and Troian velocity slip for the flow of ternary nanofluid past a stretching sheet. *Scientific Reports*, *13*(1). https://doi.org/10.1038/s41598-023-29485-0

Lund, L. A., Omar, Z., Khan, I., & Sherif, E. S. M. (2020). Dual solutions and stability analysis of a hybrid nanofluid over a stretching/shrinking sheet executing MHD flow. *Symmetry*, *12*(2). https://doi.org/10.3390/sym12020276

Manjunatha, S., Puneeth, V., Gireesha, B. J., & Chamkha, A. J. (2022). Theoretical Study of Convective Heat Transfer in Ternary Nanofluid Flowing past a Stretching Sheet. *Journal of Applied and Computational Mechanics*, *8*(4), 1279–1286. https://doi.org/10.22055/JACM.2021.37698.3067

Mishra, A. (2024). Significance of Thompson and Troian slip effects on Fe3O4-CoFe2O4 ethylene glycol-water hybrid nanofluid flow over a permeable plate. *Hybrid Advances*, *6*, 100262. https://doi.org/10.1016/j.hybadv.2024.100262

Mwamba, N. (2024). Powell-Eyring Nanofluid Flow over a Stretching Sheet. *Applied and Computational Mathematics*, *13*(5), 153–164. https://doi.org/10.11648/j.acm.20241305.14

Naseem, T., Bibi, I., Shahzad, A., & Munir, M. (2023). Analysis of Heat Transport in a Powell-Eyring Fluid with Radiation and Joule Heating Effects via a Similarity Transformation. *Fluid Dynamics and Materials Processing*, *19*(3), 663–677. https://doi.org/10.32604/fdmp.2022.021136

Oke, A. S., & Mutuku, W. N. (2021). Significance of viscous dissipation on MHD Eyring–Powell flow past a convectively heated stretching sheet. *Pramana*, *95*(4), 199. https://doi.org/10.1007/s12043-021-02237-3

Pal, D., & Mondal, S. K. (2022). Magneto-bioconvection of Powell Eyring nanofluid over a permeable vertical stretching sheet due to gyrotactic microorganisms in the presence of nonlinear thermal radiation and Joule heating. *International Journal of Ambient Energy*, *43*(1), 924–935. https://doi.org/10.1080/01430750.2019.1679253

Patel, M., & Timol, M. G. (2009). Numerical treatment of Powell–Eyring fluid flow using Method of Satisfaction of Asymptotic Boundary Conditions (MSABC). *Applied Numerical Mathematics*, *59*(10), 2584–2592. https://doi.org/10.1016/j.apnum.2009.04.010

Qasim, M., Ali, Z., Wakif, A., & Boulahia, Z. (2019). Numerical Simulation of MHD Peristaltic Flow with Variable Electrical Conductivity and Joule Dissipation Using Generalized Differential Quadrature Method. *Communications in Theoretical Physics*, *71*(5), 509–518. https://doi.org/10.1088/0253-6102/71/5/509

Rahimi, J., Ganji, D. D., Khaki, M., & Hosseinzadeh, K. (2017). Solution of the boundary layer flow of an Eyring-Powell non-Newtonian fluid over a linear stretching sheet by collocation method. *Alexandria Engineering Journal*, *56*(4), 621–627. https://doi.org/10.1016/j.aej.2016.11.006

Ramireddy, P., & Lakshmi, K. J. (2024). Thermally Stratified Flow of Powell Eyring Hybrid Nanofluid with Joule Heating Over a Porous Stretching Sheet. *JP Journal of Heat and Mass Transfer*, *37*(6), 759–789. https://doi.org/10.17654/0973576324048

Ramzan, M., Chung, J. D., Kadry, S., Chu, Y. M., & Akhtar, M. (2020). Nanofluid flow containing carbon nanotubes with quartic autocatalytic chemical reaction and Thompson and Troian slip at the boundary. *Scientific Reports*, *10*(1). https://doi.org/10.1038/s41598-020-74855-7

Rashad, A. M., Nafe, M. A., & Eisa, D. A. (2023). Heat Generation and Thermal Radiation Impacts on Flow of Magnetic Eyring–Powell Hybrid Nanofluid in a Porous Medium. *Arabian Journal for Science and Engineering*, *48*(1), 939–952. https://doi.org/10.1007/s13369-022-07210-9

Raza, J. (2019). Thermal radiation and slip effects on magnetohydrodynamic (MHD) stagnation point flow of Casson fluid over a convective stretching sheet. *Propulsion and Power Research*, *8*(2), 138–146. https://doi.org/10.1016/j.jppr.2019.01.004

Roşca, A. V., & Pop, I. (2013). Flow and heat transfer over a vertical permeable stretching/shrinking sheet with a second order slip. International Journal of Heat and Mass Transfer, 60(1), 355–364. https://doi.org/10.1016/j.ijheatmasstransfer.2012.12.028

Saidur, R., Leong, K. Y., & Mohammed, H. A. (2011). A review on applications and challenges of nanofluids. *Renewable and Sustainable Energy Reviews*, *15*(3), 1646–1668. https://doi.org/10.1016/j.rser.2010.11.035

Salleh, M. Z., Nazar, R., & Pop, I. (2010). Boundary layer flow and heat transfer over a stretching sheet with Newtonian heating. *Journal of the Taiwan Institute of Chemical Engineers*, *41*(6), 651–655. https://doi.org/10.1016/j.jtice.2010.01.013

Schlichting, H., & Gersten, K. (2016). Boundary-Layer Theory. In *Boundary-Layer Theory*. Springer Berlin Heidelberg. https://doi.org/10.1007/978-3-662-52919-5

Shampine, L. F., & Kierzenka, J. (2000). *Solving Boundary Value Problems for Ordinary Differential Equations in MATLAB with bvp4c*.

Sheikholeslami, M., & Ganji, D. D. (2016). Magnetohydrodynamic and ferrohydrodynamic. In *External Magnetic Field Effects on Hydrothermal Treatment of Nanofluid* (pp. 1–47). Elsevier. https://doi.org/10.1016/B978-0-323-43138-5.00001-X

Sher Akbar, N., Ebaid, A., & Khan, Z. H. (2015). Numerical analysis of magnetic field effects on Eyring-Powell fluid flow towards a stretching sheet. *Journal of Magnetism and Magnetic Materials*, *382*, 355–358. https://doi.org/10.1016/j.jmmm.2015.01.088

Simpson, R. L. (1989). Turbulent Boundary-layer Separation. In *Ann. Rev. Fluid Mech* (Vol. 21). www.annualreviews.org

Singh, B., Sood, S., Thakur, A., & Chandel, S. (2024). Numerical analysis of mixed convection and Thomson-Troian slip effects on ternary nanofluid flow and heat transfer over a stretching sheet with porous media: Darcy-Forchheimer model. *Applied and Computational Mechanics*, *18*(2). https://doi.org/10.24132/acm.2024.894

Smith, F. T. (1986). Steady and Unsteady Boundary-Layer Separation. *Annual Review of Fluid Mechanics*, *18*(1), 197–220. https://doi.org/10.1146/annurev.fl.18.010186.001213

Sochi, T. (2011). *Slip at Fluid-Solid Interface*. https://doi.org/10.1080/15583724.2011.615961

Ullah, H., Khan, I., Fiza, M., Hamadneh, N. N., Fayz-Al-Asad, M., Islam, S., Khan, I., Raja, M. A. Z., & Shoaib, M. (2021). MHD Boundary Layer Flow over a Stretching Sheet: A New Stochastic Method. In *Mathematical Problems in Engineering* (Vol. 2021). Hindawi Limited. https://doi.org/10.1155/2021/9924593

Uthe, B., Sader, J. E., & Pelton, M. (2022). Optical measurement of the picosecond fluid mechanics in simple liquids generated by vibrating nanoparticles: a review. *Reports on Progress in Physics*, *85*(10), 103001. https://doi.org/10.1088/1361-6633/ac8e82

Yahya, A. U., Salamat, N., Huang, W. H., Siddique, I., Abdal, S., & Hussain, S. (2021). Thermal charactristics for the flow of Williamson hybrid nanofluid (MoS2 + ZnO) based with engine oil over a streched sheet. *Case Studies in Thermal Engineering*, *26*. https://doi.org/10.1016/j.csite.2021.101196

Zheng, L., & Zhang, X. (2017). Modeling and Analysis of Modern Fluid Problems. In *Modeling and Analysis of Modern Fluid Problems* (pp. 1–37). Elsevier. https://doi.org/10.1016/B978-0-12-811753-8.00001-3

APPENDICES

MATLAB coding

```
function CodingFYP

format long g

%Define all parameters
global phi_1 phi_2 phi_3 Pr lambda A1 A2 A3 A4 A5 B E L1 L2 M S

%Boundary layer thickness & stepsize
etaMin = 0;
etaMax1 = 25; %blt 1st solution 20
etaMax2 = 25; %blt 2nd solution 20
stepsize1 = etaMax1;
stepsize2= etaMax2;

% Input for the parameters
phi_1 = 0; phi_2 = 0; phi_3 = 0; % Nanoparticle volume fraction
Pr = 30;  % Prandtl number Engine oil
lambda = -1; % moving parameter
B = 0.5; E = 0.8; % Eyring powell fluid parameter
L1 = 0.5; L2 = 0.5; % Slip velocity parameter and critical shear rate
M = 0.2; % Magnetic parameter
S = 2.5; % Suction parameter

C_1 = 893; rho_1 = 2720; k_1 = 222; s_1 = 34.83*(10^6); % AA7072
C_2 = 960; rho_2 = 2810; k_2 = 173; s_2 = 26.77*(10^6); % AA7075
C_3 = 700; rho_3 = 4907; k_3 = 3.7; s_3 = 5.51*(10^9); % CobaltFerrite
C_f = 1910; rho_f = 884; k_f = 0.144; s_f = 2.1*(10^(-12)); % Engine oil

s_nf = s_f*((s_3*(1+2*phi_3)+s_f*(1-2*phi_3))/(s_3*(1-phi_3)+s_f*(1+phi_3)));
s_hnf = s_nf*(s_2*(1+2*phi_2)+s_nf*(1-2*phi_2))/(s_2*(1-phi_2)+s_nf*(1+phi_2));
s_thnf = s_hnf*(s_1*(1+2*phi_1)+s_hnf*(1-2*phi_1)*phi_1+s_2*phi_2)/(s_1*(1-phi_1)↙
+s_hnf*(1+phi_1));

k_nf = k_f*((2*k_f+k_3-2*phi_3*(k_f-k_3))/(k_3+2*k_f+phi_3*(k_f-k_3)));
k_hnf = k_nf*((2*k_nf+k_2-2*phi_2*(k_nf-k_2))/(k_2+2*k_nf+phi_2*(k_nf-k_2)));
k_thnf = k_hnf*((k_1+2*k_hnf-2*phi_1*(k_hnf-k_1))/(k_1+2*k_hnf+phi_1*(k_hnf-k_1)));

A1 = 1/((1-(phi_1+phi_2+phi_3))^2.5);
A2 = s_thnf/s_f;
A3 = ((1-phi_2)*((1-phi_2)*((1-phi_3)*rho_f+phi_3*rho_3)+phi_2*rho_2)+phi_1*rho_1)↙
/rho_f;
A4 = k_thnf/k_f;
A5 = ((rho_1*C_1*phi_1)+(1-phi_1)*((1-phi_2)*((1-phi_3)*(rho_f*C_f))+phi_3*rho_2*C_2))/↙
(rho_f*C_f);

%%%%%%%%%%%%%%%%%%%%%%%%   first solution   %%%%%%%%%%%%%%%%%%%%%%%%%%%%%%%%%%

    options = bvpset('stats','off','RelTol',1e-10);
    solinit = bvpinit (linspace (etaMin, etaMax1, stepsize1), @OdeInit1);
    sol = bvp4c (@OdeBVP, @OdeBC, solinit, options);
```

```
  eta = linspace (etaMin, etaMax1, stepsize1);
  y = deval (sol, eta);

  figure(1)
  plot(sol.x,sol.y(2,:),'r')
  xlabel('\eta')
  ylabel('f`(\eta)')
  hold on

  figure(2)
  plot(sol.x,sol.y(4,:),'r')
  xlabel('\eta')
  ylabel('t(\eta)')
  hold on

  %Saving the output in txt file for first solution
  descris = [sol.x; sol.y];
  save 'upper.txt' descris -ascii

  %Displaying the output for first solution
  fprintf('\nFirst solution:\n');
  fprintf('f"(0) = %7.9f\n',y(3));
  fprintf('-t`(0) = %7.9f\n',-y(5));
  fprintf('skin friction = %7.9f\n',(A1+B)*y(3)-(B*E/3)*(y(3))^3);
  fprintf('Nusselt Number = %7.9f\n',-A4*y(5));
  fprintf('\n');

%%%%%%%%%%%%%%%%%%%%%%   second solution   %%%%%%%%%%%%%%%%%%%%%%%%%%%%%%%%

  options = bvpset('stats','off','RelTol',1e-10);
  solinit = bvpinit (linspace (etaMin, etaMax2, stepsize2), @OdeInit2);
  sol = bvp4c (@OdeBVP, @OdeBC, solinit, options);
  eta = linspace (etaMin, etaMax2, stepsize2);
  y = deval (sol, eta);

  figure(1)
  plot(sol.x,sol.y(2,:),'--r')
  xlabel('\eta')
  ylabel('f`(\eta)')
  hold on

  figure(2)
  plot(sol.x,sol.y(4,:),'--r')
  xlabel('\eta')
  ylabel('t(\eta)')
  hold on

  %Saving the output in txt file for second solution
  descris = [sol.x; sol.y];
  save 'lower.txt' descris -ascii
```

```
    %Displaying the output for second solution
    fprintf('\nSecond solution:\n');
    fprintf('f"(0) = %7.9f\n',y(3));
    fprintf('-t`(0) = %7.9f\n',-y(5));
    fprintf('skin friction = %7.9f\n',(A1+B)*y(3)-(B*E/3)*(y(3))^3);
    fprintf('Nusselt Number = %7.9f\n',-A4*y(5));
    fprintf('\n');

%%%%%%%%%%%%%%%%%%%%%%%%%%%%%%%%%%%%%%%%%%%%%%%%%%%%%%%%%%%%%%%%%%%%%%%%%%%%%%%

%Define the ODE function
function ff = OdeBVP (x, y, Pr, A1, A2, A3, A4, A5, B, E, M)

global Pr A1 A2 A3 A4 A5 B E M

 ff = [y(2)
       y(3)
       (A2*M*y(2)+A3*((y(2))^2)-y(1)*y(3))/(A1+B-E*B*(y(3))^2)
       y(5)
       -Pr*A5*y(1)*y(5)/(A4)];

%Define the boundary condition
function res = OdeBC (ya, yb, lambda, L1, L2, S)

global lambda L1 L2 S
res = [ ya(1)-S
        ya(2)-lambda-L1*((1-L2*ya(3))^(-1/2))*ya(3)
        ya(4)-1
        yb(2)
        yb(4)];

%Setting the initial guess for first solution
function v = OdeInit1 (x, lambda, L1, L2)

global lambda L1 L2
    v =[-exp(-x)
       exp(-x)
       exp(-x)
       exp(-x)
       exp(-x)];

%Setting the initial guess for second solution
function v1 = OdeInit2 (x, lambda, L1, L2)

global lambda L1 L2


  v1 = [-exp(-x)+0.9
     0
    -0.1
    0
    4];
```